Int. J. Electrochem. Sci., 3 **(2008)** 1425 - 1462

International Journal of ELECTROCHEMICAL SCIENCE
www.electrochemsci.org

The Oxygen Evolution Reaction on Passive Oxide Covered Transition Metal Electrodes in Alkaline Solution Part II - Cobalt

Michael E. G Lyons[*], *Michael P Brandon*

Physical and Materials Electrochemistry Laboratory, University of Dublin, Trinity College, Dublin 2, Ireland
[*]E-mail: melyons@tcd.ie

Received: 21 October 2008 / *Accepted:* 6 November 2008 / *Published:* 17 November 2008

Details are outlined of an electrochemical investigation of the oxygen evolution reaction (OER) at passive oxide covered polycrystalline Co electrodes in aqueous alkaline solution. Kinetic studies on electrodes subjected to different pre-treatment routines, yielded different values of the Tafel slope and the reaction order with respect to OH^- activity. Only one mechanistic pathway could account for all observed values of these kinetic parameters. This pathway is similar, although not identical, to that proposed, in the first paper of this series, for the reaction at oxide covered Ni anodes. Using cyclic voltammetry it was shown that the mechanism for the initial passivation of Co electrodes varies with OH^- concentration. This in turn can have an effect on the experimental value of the OER Tafel slope, a phenomenon which can be rationalized in terms of a dual energy barrier model.

Keywords: oxygen evolution electrocatalysis, oxidized cobalt electrodes, transition metal electrochemistry, oxygen evolution mechanisms, dual barrier model

1. INTRODUCTION

The current article constitutes the middle instalment of a three part series of papers, which details a body of work, aimed at obtaining a consistent understanding of the oxygen evolution behaviour of passive oxide covered electrodes of the adjacent first row transition metals; Fe, Co and Ni. The underlying motivations for this study were outlined in the first paper [1]. In that article, there is provided, a description and analysis of the use of steady state polarisation measurements, electrochemical impedance spectroscopy (EIS), cyclic voltammetry (CV) and active surface area estimation techniques, in probing the kinetics of the OER at polycrystalline Ni electrodes in alkaline

solution. The present article details the application of the same techniques to the investigation of the reaction at anodic oxide covered polycrystalline Co anodes. In the concluding part of the series, attention will be devoted to Fe electrodes, and also discussed, will be the relative activities of the passive oxides of the three metals for the OER.

In contrast to the significant body of work that exists on the OER at Ni anodes, we have found only one comprehensive [2, 3] and two less detailed [4, 5] reports on the reaction mechanism at Co electrodes. The authors of two of the aforementioned works [2, 5] propose (different) modified Krasil'shchikov reaction schemes, on the basis of their experimental electrochemical kinetic data. Recall, from the first article of the present series, that the most general form of the OER reaction mechanism originally due to Krasil'shchikov [6] can be written as:

$$S + OH^- \rightarrow SOH + e^- \quad \text{(A I)}$$
$$SOH + OH^- \rightarrow SO^- + H_2O \quad \text{(A II)}$$
$$SO^- \rightarrow SO + e^- \quad \text{(A III)}$$
$$2SO \rightarrow 2S + O_2(g) \quad \text{(A IV)}$$

where, S represents a catalytically active site for the reaction.

This preference for reaction mechanisms of the Krasil'shchikov family, in the description of the OER on cobalt(-oxide) electrodes, mirrors the situation that prevails in the established literature regarding the reaction at nickel(-oxide) anodes. However, in a rigourous study [1], during which, particular emphasis was placed on the determination of reproducible [OH^-] reaction order data, we found that the Krasil'shchikov pathway is *not* suggested for the OER at passive oxide covered Ni electrodes in aqueous alkaline solution, despite its popularity in the literature. In view of the aforementioned, we set about ascertaining, whether this is also the case for Co anodes, and whether the *physisorbed peroxide* type mechanism that we favour for the OER at Ni electrodes [1] is also viable for the reaction at a passive oxide covered Co surface.

2. EXPERIMENTAL PART

2.1. General comments

Much of the experimental details are identical to those outlined in our previous article [1] on the OER at Ni electrodes, and it is therefore unnecessary to repeat them in any great detail. As before, a standard three electrode cell arrangement was employed. All electrolyte solutions were prepared from NaOH pellets (BDH AnalaR®, minimum 98% purity) using millipore water (resistivity > 18 MΩcm). No excess salts were added and all experiments were conducted at 25 ± 1°C. The electrochemical measurements were again conducted using the Zahner Elektrik IM6 Impedance measurement unit (with its in-built frequency response analyser (FRA) for impedance measurements) interfaced to a personal computer. Complex non-linear least squares (CNLS) fitting of raw impedance data to equivalent circuit models was conducted using the SIM module of the IM6 Thales software

suite. Electrode roughness factors were estimated using the OH_{ads} desorption method of Ho and Piron [6] – a schematic diagram of the appartus for such measurements was also included in the previous article [1].

2.2. Electrode preparation and pre-treatment

One point that does require explicit discussion is the preparation and pre-treatment of the working electrodes. The electrodes were prepared from a polycrystalline Co wire, diameter 2mm, purity 99.9+%, as supplied by Aldrich. An appropriate length of wire was cut, and the cross section was filed back until a flat circular surface was achieved (geometric area = 0.0314 cm^2). The piece of wire was then washed with copious de-ionised water, polished thoroughly with a slurry of 0.05 micron alumina powder, degreased with acetone, and washed again with de-ionised water. Following this, a length of copper wire was wrapped around one end of the electrode metal wire using a pliers. Conductive epoxy (Circuit Works (CW2400)) was applied to the junction between the two wires, to guarantee good ohmic contact. When this bond had matured, the wire was completely sealed, using epoxy (Araldite®), into a regular vertical glass tube, with care taken to ensure that the circular disk of metal to be exposed was in line with the end of the tube. Following the hardening of the epoxy, it was polished back, using fine grit paper, to expose the circular metal surface. This surface was polished successively with 1200 grit carbimet paper and an alumina slurry until a "mirror bright" finish was achieved.

Experiments were performed on Co electrodes subjected to three different pre-treatment regimes. For clarity these will be referred to as Co electrode "types" A – C, where we define:

- Type A: Here a Bright electrode was polished in a slurry of 0.05 micron alumina powder, rinsed in de-ionised water and used directly in this condition.
- Type B: This refers to what will later be described as an "extremely aged" Co electrode. This is a Co electrode that has been electrochemically aged by its use in many (> 40) OER polarization experiments, at high anodic potentials. Although the electrode has a "bright" appearance similar to Type A, it will be shown that its characteristic CV is somewhat different, and that it yields different values of experimental kinetic parameters in OER steady state polarisation measurements. Before use "type" B electrodes were polished in the same manner as "type" A electrodes.
- Type C: Here a bright electrode was polished as for A, but was then *pre-reduced* at –1.15 V(vs. Hg/HgO, 1M NaOH) for a period of 5 minutes in 1.0 M NaOH. Referring to Fig. 1 and the discussion of the next section, it can be seen that this potential is associated with the reduction of Co(II) oxide species and is just anodic to the potentials associated with significant hydrogen evolution. Following this the electrode was allowed to rest on open circuit for 10 minutes, before being cycled once between –1.22 V and 0.6 V at 40 $mVdec^{-1}$ (anodic direction first).

2.3. Reference electrode

A mercuric-mercuric oxide reference electrode (Radiometer Analytical, cat no. XR400) was used throughout the present study. As we have previously discussed [1], the equilibrium oxygen electrode potential is is 0.303 V vs. Hg/HgO in the same solution. It is common practice in the literature [2, 7, 8] on the OER, to express potential in terms of the oxygen overpotential, η, when the reference electrode is a Hg/HgO electrode in the same solution as the working anode. In this case η is related to the voltage E_{meas} measured on the Hg/HgO scale as follows:

$$\eta = E_{meas} - 0.303 \text{ V (at 25ºC)} \quad (1)$$

For the sake of consistency it was elected to use Hg/HgO, 1M NaOH, as the universal reference standard in this work. It is therefore appropriate to plot polarisation curves on an oxygen overpotential, η, scale, in cases where all the data has been recorded in 1.0 M NaOH solution. This approach is useful for comparing the OER catalytic performance of an electrode, with that of other anodes reported in the literature.

When used in NaOH solutions of different concentrations, the potential of the Hg/HgO electrode was checked relative to a second Hg/HgO, 1 M NaOH electode, both before and after the experiment. No significant potential drift was noted after such experiments, implying that the concentration of the NaOH in the reference electrode chamber remains effectively constant over the time scale of typical polarisation measurements (ca. 2 – 3 hours). In any case, the 1M NaOH solution in the reference electrode, was changed regularly to ensure experimental consistency. Graphs containing data recorded in electrolyte solutions other than 1.0M NaOH, are plotted in terms of the potential, E, vs. Hg/HgO, 1M NaOH. Finally it is noted that a platinum wire electrode (CH Instruments, Inc. -catalogue no. CHI 115) was employed as the counter electrode.

3. RESULTS AND DISCUSSION

3.1. The electrochemistry of cobalt electrodes in aqueous alkaline solution

A prominent theme in our previous article on the OER at passive oxide covered Ni electrodes, was the influence of the oxide properties on the electrode catalytic activity. To understand the OER at a particular oxide electrode, it is essential to understand the surface electrochemistry of that oxide. In light of this, a short review is now provided, on the nature of the passive oxide formed on Co electrodes in alkaline solution.

Much of our knowledge on the passivation of metallic Co is derived from voltammetric studies – the results of subjecting an initially bright “type” A Co electrode to repetitive potential cycling in 1.0 M NaOH are depicted in Fig. 1.

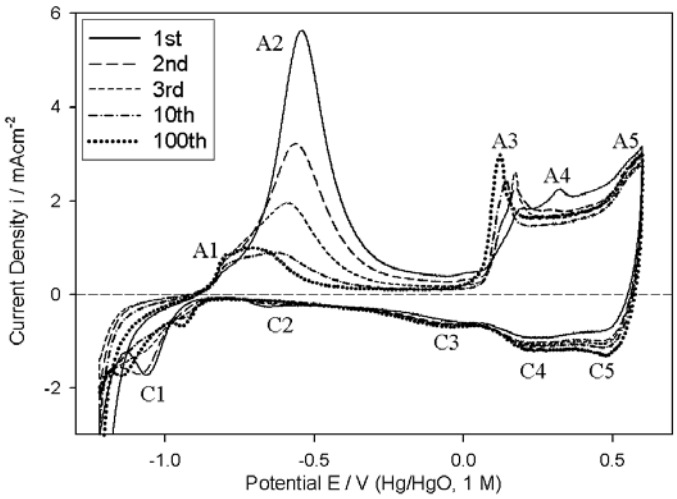

Figure 1. Analytical cyclic voltammograms (CVs) (cycle number as indicated in the legend), recorded at 40 mVs^{-1}, of an initially bright, fresh, polycrystalline (i.e. "type"A) Co electrode in 1M NaOH solution. All CVs were recorded between –1.22 V and 0.6 V at 25°C. The intervening cycles were performed between the same limits at 300 mVs^{-1}.

These voltammograms are very similar in appearance to others presented in the literature for this system [5, 9-13]. Regarding the interpretation of the various peaks in such CVs, there appears to be fairly good general agreement between the various workers who have tackled this problem [5, 9-13]. The approach adopted in most of the latter works is based on that of Behl and Toni [9] who compared the observed peak potentials with thermodynamic data. Thus, peak A1 is attributed to the formation of adsorbed OH species on the electrode surface:

$$Co + OH^- \rightarrow CoOH_{ads} + e^- \quad (2)$$

The major peak, A2, is attributed to a combination of the formation of a passivating film of $Co(OH)_2$ and/or CoO:

$$Co + 2OH^- \rightarrow Co(OH)_2 + 2e^- \quad (3)$$

$$Co + 2OH^- \rightarrow CoO + H_2O + 2e^- \quad (4)$$

and, on the basis of the results of ring disk electrode measurements [9], a dissolution process forming a soluble Co(II) species, possibly [5] $CoO{\cdot}OH^-$:

$$Co + 2OH^- \rightarrow CoO.OH(aq) + H^+ + 2e^- \quad (5)$$

With repetitive potential cycling, it is obvious that the magnitude of peak A2 decreases, while the peak potential shifts to more negative values. While the charge associated with peak A2 is observed to decrease over the first three cycles, the magnitude of the corresponding broad cathodic peak C2 is observed to remain approximately invariant. Šimpraga [12] noted that the ratio of the

charges associated with this set of corresponding anodic and cathodic peaks in 0.5M NaOH at 298 K, became unity after ca.15 cycles in the potential range of approximately –1.125 to -0.325 V (vs. Hg/HgO). Similar observations were made by other workers [5, 13, 14]. This behaviour has been attributed to the stabilisation of the developing anodic film with respect to the dissolution process of (5), so that after a number of cycles the anodic peak in the potential region of –0.6 to –0.8 V (Hg/HgO) should be almost entirely due to a solid state process.

The rather poorly distinguished peaks A3 and A4 are attributed to the oxidation of Co(II) species to Co(III) species. Burke and co-workers [5] commented that in view of the large background currents in the region of these peaks, the likelihood is that a *hydrous* Co(II) film is gradually converted to Co(III) containing species such as Co_3O_4, Co_2O_3 and CoOOH. They point out that, the situation is further complicated by a number of other factors, such as the existence of three forms of CoOOH, i.e. CoOOH(I), CoOOH(II) and $CoHO_2$. Gomez Meier et al.[11] also allude to the complex hydrous nature of the anodic oxide formed on Co in alkaline solution. These authors view the oxide growth process in terms of the formation of "sandwich-type" structures, with a Co/CoO/$Co(OH)_2$ "sandwich" formed at ower potentials. They then envisage the oxidation of a hydrous form of this "sandwich" to form a new hydrated "sandwich" structure at more positive potentials (peak A3), according to the process,

$$\left[Co(CoO)(CoOOH.xH_2O)\right] \rightarrow \left[Co(CoO)(CoOOH.yH_2O)\right] + H^+ + zH_2O + e^- \qquad (6)$$

where z=x+y. The nature of the "sandwich" will further change with increasing potential, with the CoO component being oxidised to Co_3O_4. According to this viewpoint, peak A4 will then correspond to a process along the lines of:

$$\left[Co(Co_3O_4.CoOOH)\right] + 2H_2O \rightarrow \left[Co(CoOOH)_4\right] + H^+ + e^- \qquad (7)$$

Ellipsometry measurements [15, 16], on electrochemically generated passive films on Co in alkaline solution, lend support to the idea of a "sandwich" structure. The most general conclusion of these studies was that cobalt forms two types of passive layers in alkaline solution. The first is formed at lower potentials, has a pH dependent thickness, and consists of $Co(OH)_2$ and CoO. A second passive layer is formed outside the Co(II) layer at potentials above ca. 0 V (vs. Hg/HgO) and is envisaged to consist of Co(III) and possibly Co(IV) species. X-ray photoelectron spectroscopy (XPS) measurements by Foelske et al.[17] on polycrystalline Co in 0.1 M NaOH, also emphasise the concept of a twin layer type passive film. Below the potential region corresponding to peak A3 in our Fig. 1, the passive layer is described as being a $Co(OH)_2$ film, which can grow to 40 nm thickness, depending on time and potential. At potentials anodic to peak A3 the outer layers of the film are said to be dominated by Co(III) species, with the XPS measurements identifying Co_3O_4 and CoOOH. The "sandwich" type model for the passivation of Co in alkaline solution is reminiscent of the duplex layer model for the metallic electrode/oxide/solution structure that was proposed by Burke and co-workers [18, 19]. In this approach the oxide film is envisaged to consist of an *inner compact anhydrous layer*, MO_x, and an *outer microdispersed hydrous layer* of the general form, $MO_a(OH)_b(OH_2)_c$. This model has been

applied by the present authors to the passivation of polycrystalline Fe electrodes in alkaline solution [20, 21].

Most workers [5, 11-13] agree that peak A5 is due to a *surface* Co(III) to Co(IV) oxidation. Mössbauer spectroscopy studies [22] have verified the view that at high anodic potentials, the outer surface of a CoOOH film is oxidised to a Co(IV) state. The relatively small amounts of charge associated with the cathodic peaks of Fig. 1 during the early potential cycles, indicates that the initially formed passivating film is not easily reduced. Peak C5 arises from the reduction of the surface Co(IV) species to the Co(III) valance state. Peak C4 and the broad ill-defined cathodic peak C3 are generally attributed to the reduction of Co(III) species [5, 9-14]. The well-defined C1 peak is associated with the reduction of Co(II) species [5, 10, 12, 13].

3.2. The variation of the initial passivation mechanism with hydroxide ion concentration

The surface redox chemistry of cobalt as a function of hydroxide ion concentration was subjected to a detailed exploration. Consequently, repetitive potential cycling experiments, identical in procedure to those depicted in Fig. 1 for 1 M NaOH, were conducted at a range of other electrolyte concentrations in order to more completely characterise the passivation of Co electrodes in aqueous alkaline media – the results are reproduced in Fig. 2. While the data presented here, may seem more relevant to an article on the (oxy-)hydroxide electrochemistry of Co, we believe that it illustrates an important aspect of the initial passivation of the metal, that will in turn assist in the interpretation of OER steady state polarisation data for Co anodes.In the case of Fig 2 (c) and (d) a broad symmetrical anodic peak (A2 if we retain the previous nomenclature), with a peak potential of ca. –550mV, is noted in the first few voltammetric cycles. The magnitude of this peak diminishes rapidly from cycle to cycle over the first number of cycles. As discussed in the previous section, this behaviour is believed to be due to a dissolution process, which is significant in the initial formation of the inner region of the passivating oxide film via a dissolution/precipitation mechanism. By the 10^{th} cycles of Fig 2 (c) and (d) the developing oxide film has apparently become stable with respect to the dissolution reaction, and the redox peak in this potential region at this stage, is principally related to the oxidation, by a solid state electrochemical process, of Co to Co(II) species, probably at the metal-oxide interface.

The key observation from the data of Figs. 1 and 2, is that, the behaviour over the course of the first few voltammetric cycles is fundamentally different for the lower concentration electrolytes as compared with the 3.0 or 5.0 M NaOH solutions. For both the 0.25 M and 0.5 M experiments (Fig 2 (a) and (b)), the magnitude of the A2 anodic peak actually increases over these early cycles, in marked contrast to the behaviour discussed in the previous paragraph. The data of Fig. 2 (a) and (b) suggest that dissolution/precipitation is largely unimportant in the initial formation of the passive oxide film on a bright Co electrode in either 0.25 or 0.5 M NaOH. As previously discussed, the evolution of the voltammetric profile of Fig. 1 with the number of cycles, points to some dissolution activity for 1.0 M NaOH – however, comparing Figs. 1 and 2(d), the dissolution current in this case is of a significantly smaller magnitude than in the case of the 5.0 M solution. Overall it can be concluded that a

dissolution/precipitation mechansim becomes progressively more significant in the initial passivation of bright Co electrodes with increasing OH^- ion concentration in the range 0.25 M ≤ [OH^-] ≤ 5.0 M.

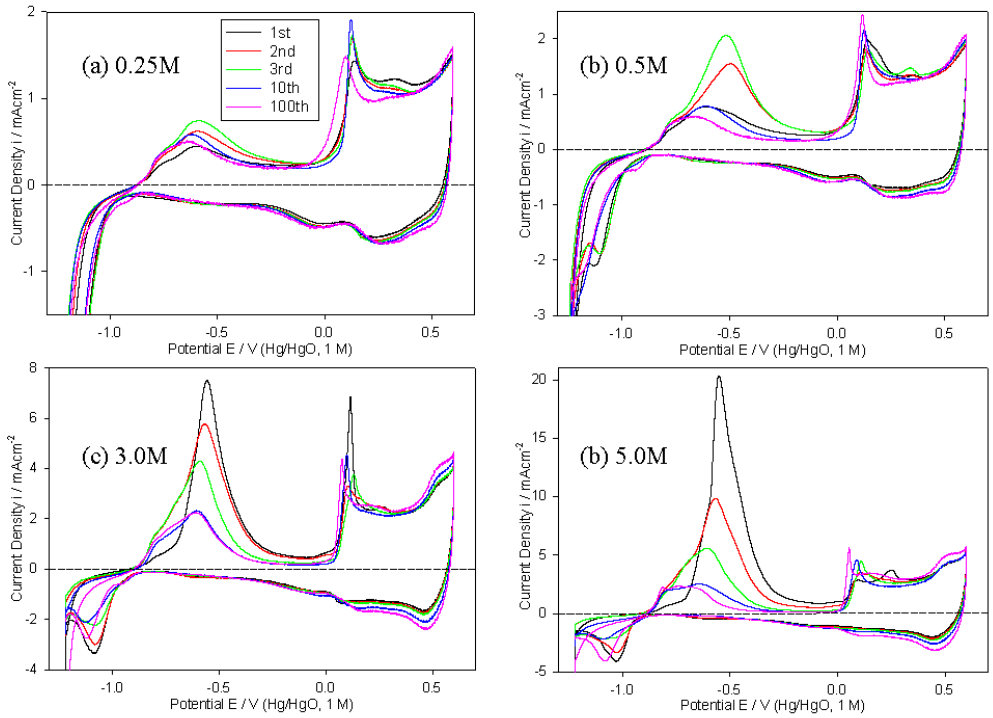

Figure 2. Analytical CVs (cycle number as indicated in the legend) recorded at 40 mVs^{-1} of a "type" A Co electrode in (a) 0.25 M, (b) 0.5 M, (c) 3M and (d) 5M solutions of NaOH. All CVs recorded between –1.22 V and 0.6 V at 25°C. The intervening cycles were performed between the same limits at a sweep rate of 300 mVs^{-1}.

The above interpretation of the voltammetric data of Figs. 1 and 2, is consistent with the previously cited ring disk electrode data of Behl and Toni [9]. These workers detected small but significant amounts of dissolved Co^{2+} species, the concentration of which reached a maximum at potentials just below those corresponding to peak A2 in our Fig 1. The amount of dissolved Co^{2+} increased with increasing KOH concentration. This data was corroborated, and added to, by a combined rotating ring disk electrode (RRDE), and scanning electrochemical microscopy (SECM) study carried out more recently by Erts et al.[23]. In their ring disk electrode experiments, they observed that ~ 3% soluble species were collected in 1M NaOH in the same potential region as Behl and Toni made their soluble species observation. No soluble species were detected at the ring in 0.1 M NaOH. According to Erts and co-workers, SECM offers a more accurate method of quantification of concentrations of soluble species since "the tip electrode can be located close to the surface and more short lived species can be detected". In 1.0 M NaOH in the potential region of peak A2, they observed that a "much larger fraction of the reaction proceeds through the dissolution/ precipitation path than revealed from RRDE". The disparity between the SECM results and the RRDE data was explained in

terms of a rapid precipitation of the soluble Co^{2+} species, with the result that much of the soluble species couldn't escape to the bulk solution and register a ring current. In 0.1 M NaOH no soluble species were detected by SECM, indicating a solid-state oxidation mechanism, in the less concentrated solution.

A final relevant point in relation to the surface electrochemistry of the passive oxide, is illustrated by the voltammetric data of Fig. 3. Examining the anodic sweep, it is evident that the rising edge of the OER current, develops from the redox peak associated with the surface Co(III) to Co(IV) oxidation process. This is analogous to the situation that prevails at anodic oxide covered Ni anodes [1] in alkaline solution, where the onset of significant OER current, appears just anodic to the Ni(II)→Ni(III) redox peak. In that case Ni(III) surface species are identified as the catalytic sites for oxygen evolution – it is therefore resonable to suggest that Co(IV) species provide the active centres for the reaction in the case of passive oxide covered Co electrodes. Tetravalent Co species have also been proposed to be the catalytically active sites towards the OER, for electrodes consisting of cobalt oxides (cobaltites) prepared by various means [24-26].

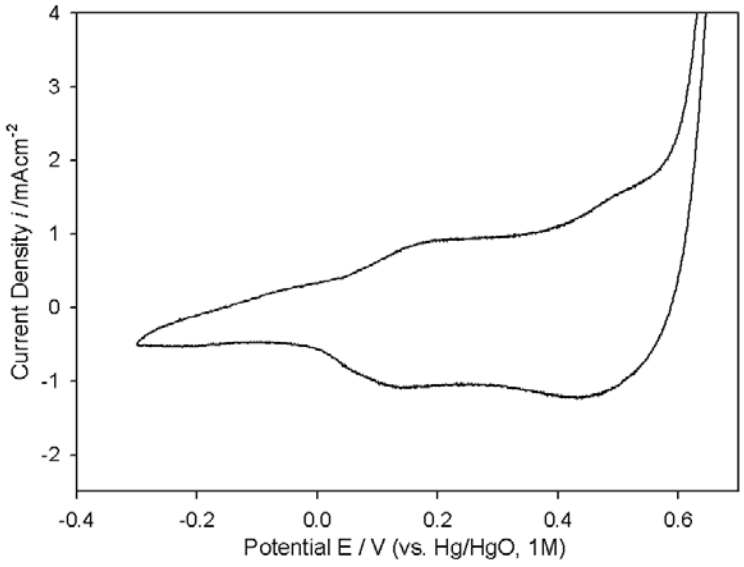

Figure 3. First voltammetric cycle of a "type" A Co electrode in 1.0 M NaOH solution (scan rate 40 mVs^{-1}), indicating that, on the anodic half cycle, the OER current rises from the Co(III)→Co(IV) oxidation peak.

3.3. Co electrode 'type' A

In contrast to our experience with Ni anodes [1], it proved possible, over the course of 10 – 15 experiments, to record OER steady state polarisation curves with satisfactory reproducibility (i.e. insignificant change in the measured value of i at a given applied E, for a solution of particular OH^- concentration) for Co electrodes that were not subjected to any pre-treatment, beyond mechanical polishing.

As discussed elsewhere [1], our approach to steady state polarisation experiments has been to record data, initially in the anodic direction over the course of several hundred mVs in the potential region of significant OER current density, before reversing the sweep direction and continuing measurement down to the potential at which the net current becomes cathodic. The results of two such experiments, with different upper reversal overpotentials, conducted on a "type" A Co electrode in 1.0 M NaOH are presented in Fig. 4. As we also observed for bi-directional OER steady state polarisation curves recorded for Ni electrodes [1], there is hysterisis at higher overpotentials between the forward and reverse scans. Furthermore, the severity of the hysterisis is evidently a function of the upper reversal potential. Similar hysterisis was observed in the polarisation curves for each of the NaOH electrolyte solution concentrations employed in the study. It is worth noting that bi-directional log$i - \eta$ plots, very similar in appearance to those of Fig. 4, were recorded by Willems, Kobussen and co-workers [2] for the OER on polycrystalline Co electrodes in KOH solutions of various concentration. In fact the only useful discussion, that we have encountered in the literature, of hysterisis effects in OER steady state polarisation data, was provided by the same workers [27], albeit for a different electrode material ($La_{0.5}Ba_{0.5}CoO_3$). Consistent with our work on Ni [1], we have taken the view, that kinetic mechanistic analysis is most reliably performed on polarisation data in regions of potential, where the forward and reverse scans are largely coincident.

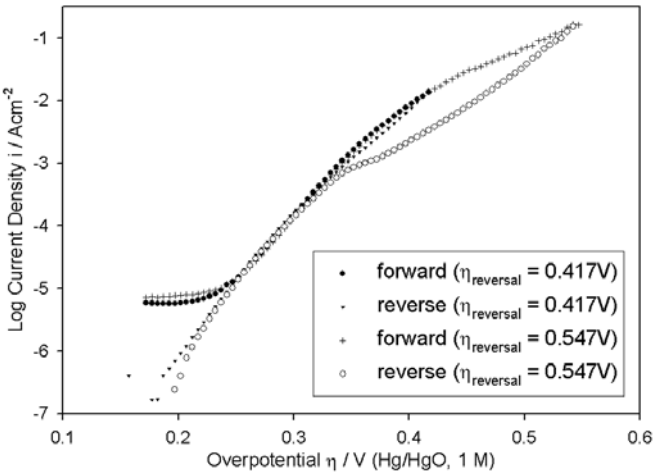

Figure 4. Comparison of two bi-directional, *iR* corrected OER steady state polarisation curves recorded for "type" A Co electrodes in 1.0 M NaOH solution, initially in the direction of increasing potential, at 25°C. The scan direction was reversed at an overpotential of 0.417 V in one experiment and at 0.547 V in the other. Otherwise all conditions were identical.

In view of this, a series of *iR* compensated steady state polarisation curves, recorded at lower oxygen evolution overpotentials (first scan in the direction of increasing potential) for "type" A electrodes are presented in Fig. 5. It is clear that the Tafel slope, *b*, increases with decreasing OH^- activity, varying from 40 mVdec^{-1} in 5.0 M NaOH to 47 mVdec^{-1} in 1.0 M NaOH. The slope of 40mVdec^{-1} observed for the 5.0 M solution, is in excellent agreement with a slope of ~ 40 mVdec^{-1}

observed for the OER at a polycrystalline Co electrode in 4.85 M KOH [2]. The Tafel slope of 47 $mVdec^{-1}$ noted in the present work, also agrees with a previous literature report [4], where b = ~46 $mVdec^{-1}$ was noted for oxygen evolution on a Co anode in 1 M KOH at room temperature.

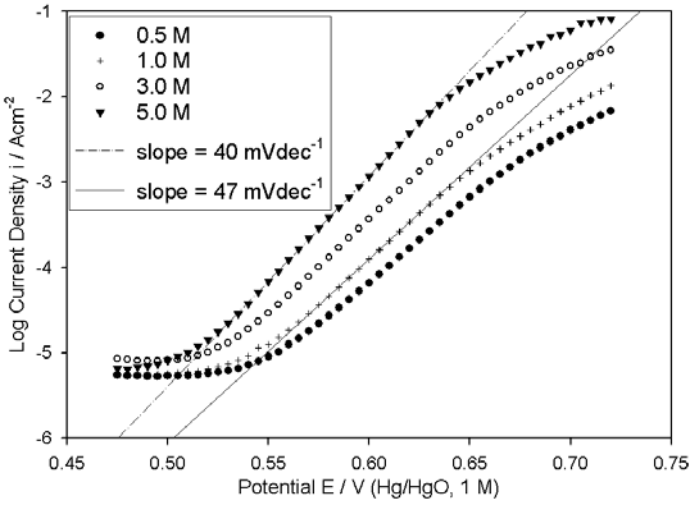

Figure 5. *iR* corrected OER steady state polarisation curves recorded in the direction of increasing potential for a "type" A Co electrode in NaOH solutions of various concentrations at 25°C.

The observed variation in b with [OH^-], implies, that for a given applied potential, the electrical contribution (via the $\exp(\alpha\eta F/RT)$ term of the Tafel equation[a]) to the reaction rate depends on the electrolyte concentration. Conventionally, a change in Tafel slope is indicative of a change in reaction mechanism, or in rate determining step (RDS) within the reaction pathway – an alternative explanation will however, be forwarded later in the article. For the moment, it is noted that a meaningful value of the OH^- reaction order, m_{OH^-}, cannot be extracted from the polarisation data of Fig. 5, owing to the aforementioned variation in b.

3.4. Co electrode 'type' C

In an attempt to circumvent the problems outlined above regarding the experimental determination of m_{OH^-}, steady state polarisation experiments were performed in various NaOH solutions (0.5 – 5.0 M), on a Co electrode subjected to pre-treatment regime C – see Fig. 6. Bi-directional polarisation curves for this "type" of Co electrode display hysterisis similar to that discussed for "type" A anodes. Significantly, values of b in the range of 46 – 49 $mVdec^{-1}$ (=~2.303×4RT/5F at 25ºC) are noted, at lower potentials, for each solution concentration in Fig. 6. Reaction order plots, constructed from these polarisation curves at two values of potential within the lower straight-line region, are presented in Fig. 7. Application of linear regression analysis to these plots, indicates an OH^- reaction order of approximately unity.

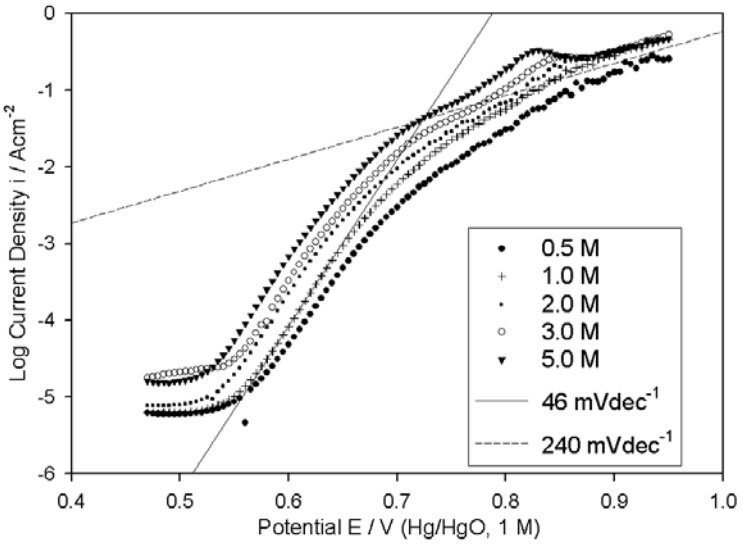

Figure 6. *iR* corrected OER steady state polarisation curves recorded in the direction of increasing potential for a "type" C Co electrode in NaOH solutions of various concentrations at 25°C.

3.5. Co electrode 'type' B

As discussed above, steady state polarisation measurements on "type" A Co electrodes yielded reproducible log$i$ – η plots, like those presented in Fig. 5, over the course of approximately 15 experiments following the initial preparation of the anode. In subsequent measurements, the value of i recorded at a given applied potential, for a given electrolyte concentration, became progressively less reproducible, while increases of ~ 3 – 5 mVdec^{-1} were noted in the values of b at all concentrations, relative to the data presented in Fig. 5. After ~30 experiments, the level of reproducibility diminished further, with, for example, different values of b, anywhere in the range of 50 - 60 mVdec^{-1}, being observed over the course of several succesive polarisation runs in 1.0 M NaOH. New limiting reproducible polarisation behaviour became obvious after ~40 experiments, with a lower overpotential Tafel slope of ~60 mVdec^{-1} being noted over a range of electrolyte concentrations.

A comparison is presented in Fig. 8, of steady state polarisation curves (1.0 M NaOH), recorded at lower oxygen evolution overpotentials for a particular Co electrode specimen, when it was freshly prepared ("type" A) and when it had become well aged ("type" B). In addition to the obvious increase in b with ageing as discussed in the previous paragraph, it is also evident, that over the range of potentials where straight line Tafel behaviour prevails, higher OER current densities are observed for the "type" B electrode relative to the fresh anode. For example, at η = 0.287 V the current density observed for the former (i = 0.207 mAcm^{-2}) is approximately 2.75 times greater than that recorded for the "type" A anode (i = 0.0753 mAcm^{-2}). Owing to the difference in Tafel slopes, the current densities for two electrodes become practically co-incident at the upper potential end of the straight-line Tafel region.

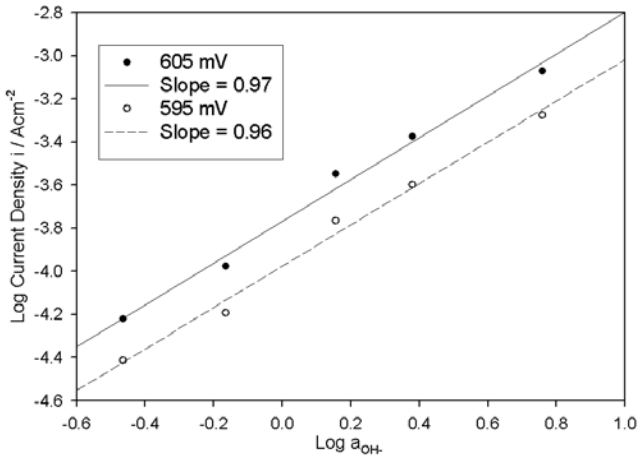

Figure 7. Reaction order plots based upon the polarisation curves of Fig. 6 at potentials of 595 and 605 mV in the ca. 46 mVdec^{-1}Tafel slope potential region.

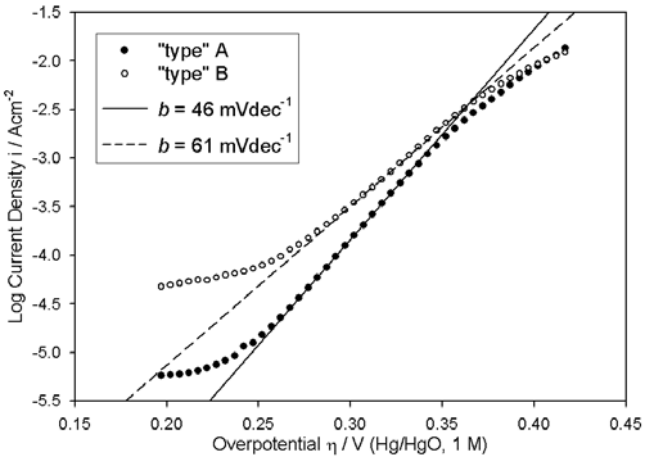

Figure 8. *iR* corrected OER steady state polarisation curves recorded in the direction of increasing potential on the same Co electrode specimen, aged to different degrees, in 1.0 M NaOH solution at 25°C.

Cyclic voltammograms, characterising the surface electrochemistry of both "type" A and B Co electrodes (again the same electrode specimen, but at different stages in its service life) are presented in Fig 9. While the profiles are similar in the Co/Co(II) potential region below –0.2 V, there is clearly a huge difference in the charge capacities associated with the Co(III) and Co(IV) potential regions. Following the practice of several literature sources [5, 7, 13], the reversibly accessible active charge capacity, Q, associated with the oxidation of Co(II) species to Co(III) and the further surface oxidation to Co(IV) species, was calculated for both of the CVs of Fig. 9, by integration of the cathodic half-cycle between the limits of – 0.4 V and the upper potential at which the net current density became negative. This analysis yielded $Q_{type\ A} = \sim 3.47$ mCcm^{-2}, compared to $Q_{type\ B} = \sim 32.0$ mCcm^{-2}.

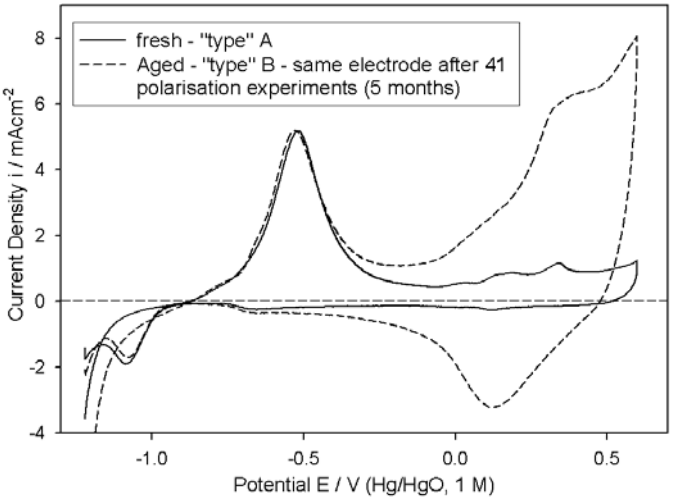

Figure 9. Cyclic voltammograms, characterising the surface electrochemistry of the initially bright Co anodes, on which the steady state polarisation curves of Fig. 8 were recorded. The above CVs were recorded in 1.0 M NaOH between –1.22 and 0.6 V, with a scan rate of 40 mVs^{-1} at 25°C.

It should be emphasised at this point, that following all polarisation experiments performed on the electrode characterised in Fig. 9, it was polished, rinsed and dried (in soft tissue paper). Unlike Ni, which retains its bright metallic finish throughout the course of oxygen evolution polarisation measurements, a dark brown coloured oxide film forms on Co, when polarised at high anodic potentials. This film was apparently readily removed by polishing, so that the electrode appeared visually similar prior to voltammetric characterisation, with a bright "mirror" finish, both when it was fresh ("type" A) and aged ("type B). However it is evident from Fig. 9, that there are significant differences in the surface electrochemistry of the two "types" of electrode. The only reasonable interpretation that we can devise for the large increase in Q with ageing, is that a residual oxide layer, resistant to removal by mechanical polishing, builds up slowly with electrode usage. It is the redox transitions of the outer regions of this film that leads to the enhancement of Q for the aged electrode relative to the fresh anode. This effect may be associated with increasing surface inhomogeneity and roughness, that would be expected to accompany the continous cycle of oxide formation in polarisation experiments, and subsequent removal by polishing. Clearly, the less smooth and homogeneous the metal surface, the more difficult is the removal of oxide adjacent to that surface by abrasive polishing techniques. In any case, we have also observed effects, that we have attributed to polishing resistant residual oxides, in the cases of Ni[1] and Fe[21] electrodes.

IR corrected OER steady state polarisation curves, recorded for a "type" B Co electrode in NaOH solutions with concentrations ranging from 0.25 – 5.0 M, are presented in Fig. 10. As discussed above, a Tafel slope of ~ 60 $mVdec^{-1}$ is evident at lower overpotentials. In addition, it is apparent that a second straight-line region exists at higher overpotentials, with a Tafel slope approximately twice that of the lower η slope. Reaction order plots, for both Tafel regions are constructed in Fig. 11. Note that the value of b, at lower overpotentials for the data recorded in the 5 M NaOH solution, is significantly less than 60 $mVdec^{-1}$, and has thus been disregarded in the graphical determination of m_{OH^-}. Poor

linearity was observed in reaction order graphs, plotted for several values of E in the upper Tafel region (including E = 0.74 V depicted in Fig. 11), however the overall (allbeit cautious) impresssion was that m_{OH^-} was smaller than for the lower Tafel range, tending to approximately unity. It can therefore be concluded, that the OER polarisation behaviour for a "type" B Co anode, is characterised by b = ~60 mVdec^{-1}, m_{OH^-} = ~3/2 at lower η, and b = ~120 mVdec^{-1}, m_{OH^-} = ~1 at higher η.

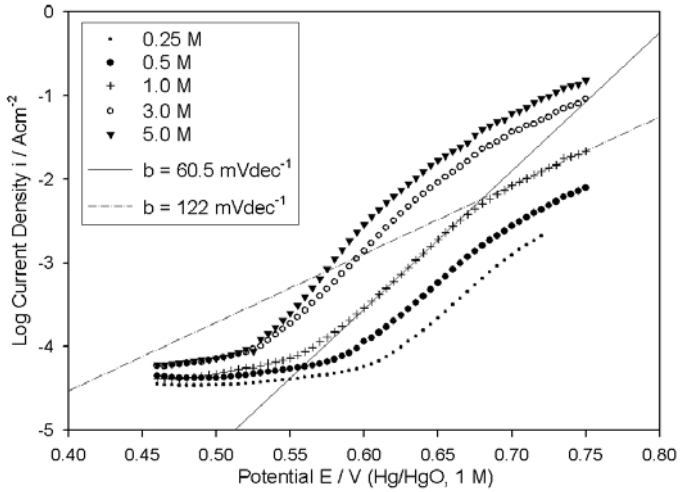

Figure 10. *iR* corrected OER steady state polarisation curves recorded in the direction of increasing potential for a "type" B Co electrode in NaOH solutions of various concentrations at 25°C.

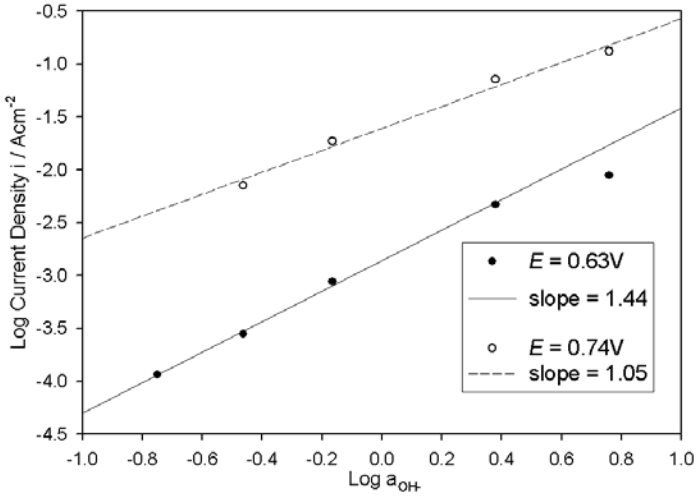

Figure 11. Reaction order plots based upon the polarisation curves of Fig. 10 at potentials of 0.630 and 0.740 V.

3.6 Electrochemical impedance spectroscopy (EIS) measurements

Electrochemical impedance data recorded for a "type" C Co electrode in 1.0 M NaOH at various potentials are presented in the Bode representation in Fig. 12, or, equivalently, in Nyquist

(complex plane) format in Fig. 13. The impedance responses of passive oxide covered Co (and indeed Ni and Fe) electrodes in the oxygen evolution potential region and the appropriate choice of equivalent circuit model will be discussed elsewhere [28] – here we restrict our treatment to aspects of the EIS data related to the kinetics of the OER and to roughness factor determination.

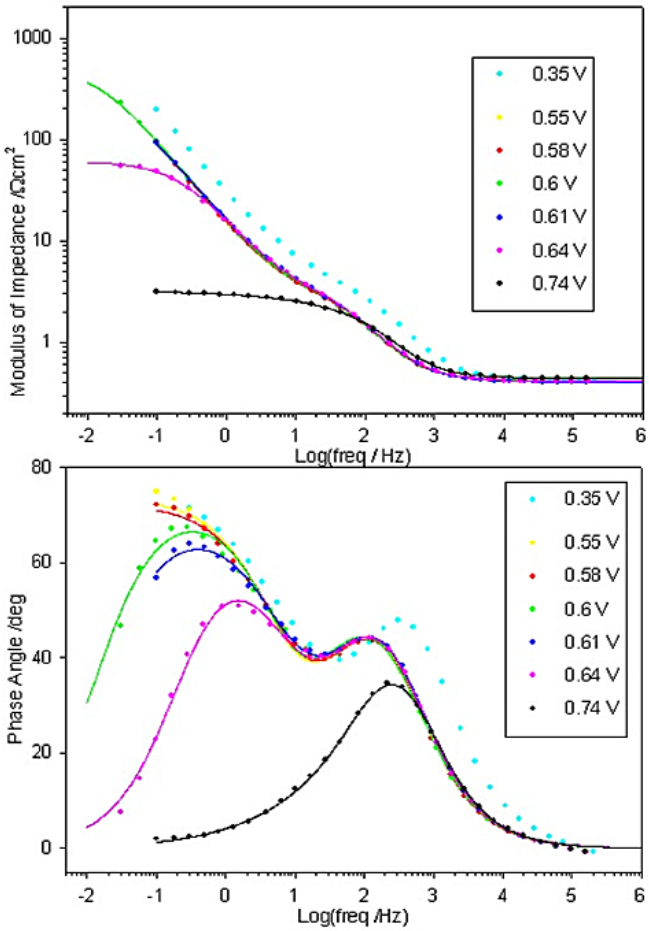

Figure 12. Bode plots recorded at various potentials for a "type" C Co electrode in 1.0 M NaOH solution at 25°C. The raw data is represented by the dots. The continuous lines are the results of CNLS fits to the equivalent circuit model of Fig. 14.

As in our analysis of impedance data for anodic oxide covered Ni electrodes in the OER potential region [1], the raw EIS data of Figs. 12/13 were fitted to the equivalent circuit model of Fig. 14 using a CNLS fitting algorithm. Recapping briefly (from our previous communication[1]) on the significance of the various circuit elements; C_{dl} models the double layer capacitance, R_Ω represents the uncompensated solution resistance, R_p and R_s are related to the interfacial charge transfer kinetics, while $C_ø$ is the value of a capacitor, which in parallel with the resistance, R_s, models correctly the relaxation of the charge associated with the adsorbed intermediate(s) [29]. Another feature common to the CNLS fitting of OER impedance spectra for Ni and Co, is the need to admit *constant phase elements* (CPEs) in place of pure capacitive elements in the equivalent circuit model, in order to

simulate frequency dispersion in the experimental capacitive response. The impedance, Z_{CPE}, of a capacitive process displaying frequency dispersion is expressed as:

$$Z_{CPE} = A(j\omega)^{-\alpha} \tag{8}$$

In equation (8), $A = 1/C_{\alpha=1}$, where $C_{\alpha=1}$ is the value of the capacitance in the absence of frequency dispersion, and α is an exponent ($\alpha \leq 1$ for a physically reasonable situation) equal to unity in the case of an ideal capacitor. The result of a CNLS fitting of raw impedance data to a CPE using the SIM program, is an output in the form of optimised values for $C_{\alpha=1}$ and α.

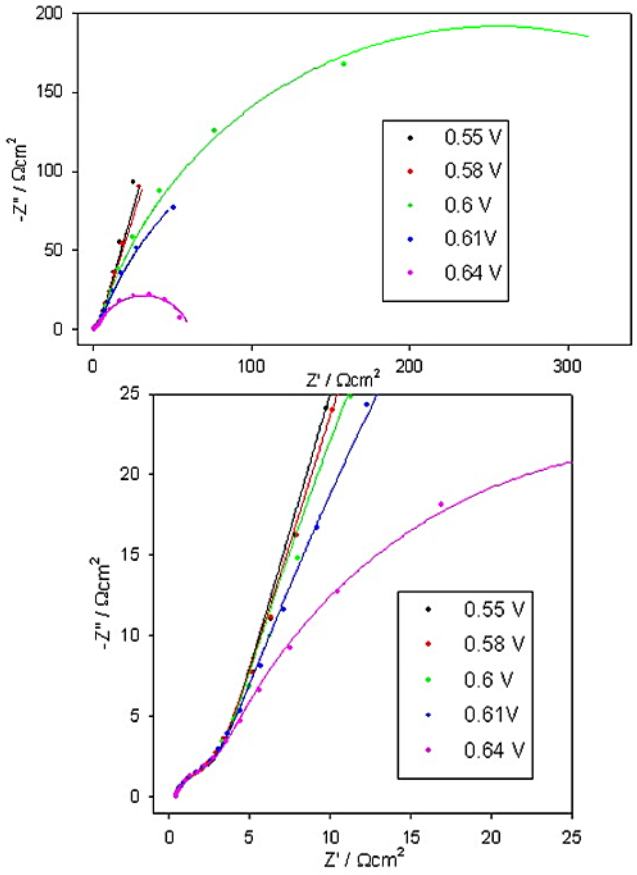

Figure 13. Nyquist representation of the impedance data presented in Fig. 12. As before, the raw data is represented by the dots, while the continuous lines are the results of CNLS fits to the circuit of Fig. 14. The lower plot is a reproduction of the higher plot at a higher resolution, with the purpose of showing the high frequency data more clearly.

The best-fit values of the equivalent circuit elements, for the CNLS fitting of the EIS data of Figs. 12/13 are listed in Table 1. The simulated impedance responses that arise from the fitting procedure are depicted as continuous lines in Figs. 12 and 13.

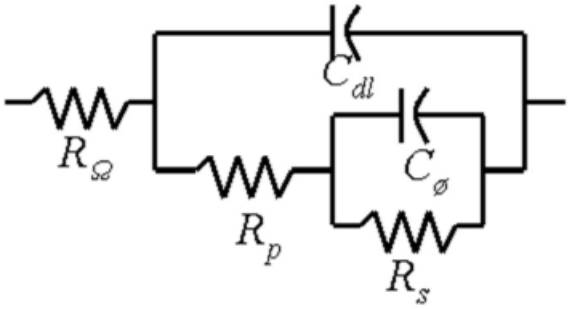

Figure 14. Equivalent circuit model used in the CNLS fitting of the impedance data of Figs. 12 and 13.

In comparison with the impedance data that we have previously presented [1] for the OER occurring at Ni anodes, there is superior temporal resolution between the high frequency ($\tau_{hf} = R_pC_{dl}$) and lower frequency ($\tau_{lf} = R_sC_\phi$) relaxation processes in the case of the "type" C Co electrode. This is manifested in Fig. 12 by the fact that two sets of maxima are evident in the phase angle vs. log frequency plot. The higher frequency set, that appear between 10^2 and 10^3 Hz, are indicative of the overall impedance response being dominated by the double-layer capacitance contribution over this frequency range. The lower frequency maxima appear at frequencies where the adsorption pseudo-capacitance is dominant. By contrast, the corresponding plot for Ni electrodes at lower OER overpotentials is characterised by one broad peak, which is in fact a superposition of the frequency dependent phase angle characteristics of the two individual relaxation processes. The observation of two distinct pseudo-semi-circular regions in the Nyquist plots of Fig. 13, compared to just one in this represenation for the EIS response of Ni anodes [1], again points to the greater difference between the low and high frequency time-constants for anodic oxide covered Co electrodes, relative to similarly passivated Ni electrodes.

Table 1. Optimum fit parameters for the CNLS fitting of the data of Figs.12/13.

E V	R_s Ωcm^2	R_s % Error	C_ϕ $mFcm^{-2}$	α	R_p Ωçm$_2$	C_{dl} µF$_2$çm^{-}	α	R_Ω Ωcm^2
0.55	------		2.484	0.820	3.955	749.94	0.825	0.412
0.58	------		2.209	0.804	3.735	746.50	0.825	0.413
0.6	503.60	22.0	2.515	0.835	4.411	729.89	0.807	0.414
0.61	407.15	24.8	1.775	0.784	3.911	695.83	0.820	0.405
0.64	56.58	3.2	2.059	0.807	4.012	699.65	0.819	0.411
0.74	1.05	2.6	1.631	0.521	1.701	596.51	0.851	0.441

This greater separation of the characteristic time constants, τ_{hf} and τ_{lf}, for Co relative to Ni electrodes, arises primarily because τ_{lf} is significantly greater for the former. This is in turn related to the fact, that for a given oxygen evolution overpotential, the adsorption pseudocapacitance as characterised by EIS measurements[b], is greater for Co than for Ni electrodes – a fact that is indicated by comparing the values of C_{ϕ} listed in Table 1, with those which we have previously reported[1] for Ni. As an example, at E = 0.6 V for the "type" C Co electrode, the optimised value of the pseudocapactive CPE is C_{ϕ} = 2.52 mFcm^{-2}, α = 0.835. For a pre-reduced Ni anode, also in 1.0 M NaOH solution, the best fit values at this potential were[1], C_{ϕ} = 67.31μFcm^{-2}, α = 0.947.

As a direct consequence of the high pseudocapacitance of the Co electrode, the total Faradaic resistance, R_F ($R_F = R_s + R_p$), is not characterised for lower overpotentials at the low frequency limit, in the case of the EIS data presented in Fig. 12. This is reflected in the % error in the fitted values of R_s listed in Table 1. The CNLS fitting program outputs an estimate of the error in the fitted value for each circuit element, based upon the difference between the experimental and calculated impedances at the frequency at which that element has its maximum significance in determining the overall measured impedance. For the optimised values of the circuit elements other than R_s, these error estimates are small (< 3%). In contrast, the fitting program found that the R_s parameter is completely meaningless for the data recorded at potentials of 0.55 and 0.58 V. It can be appreciated from Table 1, that with increasing potential, the % error in the calculated value of R_s drops as the contribution of this resistive component to the measured impedance begins to become resolved at the lowest measurement frequencies. Only at higher potentials (0.64 V) is satisfactory characterisation of R_F approached, on the timescale of these experiments. This is of course, also the reason why the lower frequency pseudo-semi-circles are only partially developed in the Nyquist plots of Fig. 13 for the lower potentials.

The reason why the high pseudocapacitance of the Co electrode, pushes the resolution of R_F to lower frequencies relative to Ni electrodes [1], is most readily explained in terms of the equivalent circuit of Fig. 14. At low frequencies the magnitude, Z_{Σ}, of the total impedance of the circuit is dominated by the R_sC_{ϕ} loop. Therefore, we can write:

$$\frac{1}{Z_{\Sigma}} \cong \frac{1}{Z_S} + \frac{1}{Z_{\phi}} = \frac{1}{R_S} + \frac{1}{\left(\omega C_{\phi}\right)^{-1}} \tag{9a}$$

Or

$$Z_{\Sigma} \cong \frac{R_S}{1 + R_S \omega C_{\phi}} \tag{9b}$$

It is clear, that as ω ($\omega = 2\pi f$, where f is the frequency of the ac perturbation) is decreased, the dominant contribution to Z_{Σ} will change from the pseudocapacitance (at frequencies where $R_s\omega C_{\phi} >> 1$) to the resistance R_s (at frequencies where $R_s\omega C_{\phi} << 1$). It is under the latter condition, that R_F can be extracted from experimental EIS data. By comparing the values listed for R_s in Table 1, with those listed for the same circuit element, in the case of a pre-reduced Ni OER anode (see ref. 1, Table 1), it is clear that R_s lies within the same order of magnitude at similar potentials, for both electrodes. In this case it is clear, that it is the relative values of C_{ϕ}, that will principally determine the frequency, for either type of electrode, below which, R_s (or more correctly R_F) becomes experimentally accessible.

The greater the magnitude of $C_{ø}$, the lower the frequencies for which $R_s\omega C_{ø} << 1$ (for similar values of R_s) – thus explaining why R_F is not resolved for the "type" C Co anode at lower η in the impedance spectra of Figs. 12 and 13, but is accessible in the case of EIS experiments carried out on a similar timescale for Ni (and indeed Fe [21]) electrodes in the same electrolyte solution.

In a trial EIS measurement [30], performed at E = 0.575 V in 1.0 M NaOH, and extended to a lower frequency of 10^{-3} Hz, it was found, that, even at this low frequency limit, R_F was not completely resolved – although with a measured phase angle of ~ 10 degrees, a reasonable estimate was possible. It must be remembered, that using FRA based EIS equipment, the time required for the acquisition of data of satisfactory quality down to a lower frequency limit of 10^{-3} Hz, is significant. While one single measurement period at 10^{-3} Hz is obviously 1000s, it is necessary to repeat this measurement over a number of periods to facilitate the integration of the impedance response. Bearing in mind, that this process must be repeated at several other measurement frequencies within the $10^{-2} – 10^{-3}$ Hz decade, it is clear that the experimental timescale would be of the order of hours at *each* measurement potential. Ageing of the oxide film on Co electrodes over such a timescale has however, been shown to affect measured OER kinetic parameters [3]. On this basis we would suggest, that FRA based impedance spectroscopy *is not a useful method* for obtaining a kinetically significant OER Tafel slope value in the case of Co electrodes in 1.0 M NaOH, despite being successfully applied to this problem in the case of Ni [1] and Fe [21] anodes in that electrolyte. Similar issues regarding the lack of resolution of R_F at the low frequency limit, arose in EIS measurements on "type" A Co electrodes in 1.0 M NaOH at lower OER overpotentials.

The question arises as to the origin of the greater pseudocapacitive response for Co, relative to Ni and Fe electrodes, at potentials associated with the lower OER linear Tafel region. A survey of the literature reveals, that just as with the data of Figs. 12 and 13, capacitive behaviour dominates the impedance responses of cobalt oxide and Co containing alloy electrodes in 1.0M OH^- solutions at lower oxygen evolution overpotentials. Kessler et al.[31] conducted EIS studies, to a lower frequency limit of 10^{-3} Hz, on the OER behaviour of the amorphous alloys G14 ($Fe_{60}Co_{20}Si_{10}B_{10}$) and G16 ($Co_{50}Ni_{25}Si_{15}B_{10}$) in 1.0M KOH. For lower overpotentials, R_F was well resolved, even at 0.1 Hz, for the G14 anode - however for G16 alloy, with its greater Co content, R_F remained poorly resolved at 10^{-3} Hz.. Wu and co-workers [32] used impedance to characterize the electrocatalytic activities for oxygen evolution, of an electrodeposited cobalt oxide phase and several Co+Ni mixed oxide phases. Nyquist representations of EIS data recorded in 1M NaOH, at a potential associated with a lower Tafel slope (b = 40 – 48 $mVdec^{-1}$ dependent on the oxide composition) region in steady state measurements, show that while R_F is well resolved for the mixed oxides at the lower frequency limit, this is not the case for the exclusively Co based oxide. Dominant capacitive responses, extending to the lowest measurement frequency, have also been reported for EIS studies at lower oxygen evolution overpotentials on, thermally prepared $NiCo_2O_4$ electrodes (1.0 M NaOH) [33], electrodeposited cobalt oxide films (1.0 M NaOH) [25] and pre-oxidised $Ni_{50}Co_{25}P_{15}B_{10}$ alloy anodes (1.0 M KOH) [34]. The most plausible explanation [25, 34] for the large capacitive response at potentials directly above the onset of significant oxygen evolution current density for cobalt oxide anodes (including our passive oxide covered Co electrodes) is that, a non-homogeneous charge distribution associated with the surface oxidation of Co(III) to Co(IV) species contributes to (and evidently dominates) the overall

pseudocapacitance, in parallel to the adsorption pseudocapacitance associated with the potential dependent coverage of OER intermediate species.

3.7. Mechanistic assignment of the OER at Co electrodes

In contrast to fresh non-pre-treated ("type" A) Co electrodes, for which b varied from ~2.303×4RT/5F in 1.0 M NaOH to ~2.303×2RT/3F in 5.0 M NaOH, it was possible to obtain a value of m_{OH^-} for pre-reduced fresh Co anodes ("type" C), as was discussed above. The experimental kinetic data recorded for "type" C electrodes (b = ~2.303×4RT/5F with associated m_{OH^-} = ~1) would therefore seem to provide a good starting point for a kinetic mechanistic determination of the operative pathway for the OER at passive oxide covered Co electrodes in alkaline solution. However a problem arises immediately, in that b = 2.303×4RT/5F is not predicted by a conventional kinetic analysis of any of the commonly cited candidate pathways for the OER, regardless of which step is chosen as rate-limiting or whether the Langmuir or Temkin isotherm is admitted to describe the potential dependent coverage of the reaction intermediates – cf. ref. 35, Table II. Such a value for b, can however be rationalised in terms of a so-called *dual barrier model*, under which it is assumed that not all of the potential difference across the metal/solution interface has a effect on the kinetics of the interfacial electron transfer reaction.

3.8. The dual barrier model

Several dual barrier models [3, 4, 36 – 43] have been outlined in the literature. Of these, we believe, that the model most relevant to the present work, is that of MacDonald and Conway [37], developed to rationalise oxygen evolution Tafel slopes of ~ 2.303×4RT/5F observed for gold electrodes in acid and alkaline solutions. This was, in turn, a development of a model, first proposed by Meyer [36] to explain very high Tafel slopes observed for cathodic processes occurring at zirconium electrodes covered by a barrier layer of ZrO_2. The model envisages that only a fraction of the total potential difference, E, between the metallic electrode and the solution is effective in charge transfer at the electrode/solution interface, with the remainder of the potential drop occurring across an electronically conductive barrier oxide layer, through which the charge passed during the course of the OER must migrate.

Applying the dual barrier model, the total applied potential, E, is expressed as $E = V_f + V_s$, where V_s is the potential affecting the normal electrochemical charge transfer barrier at the electrode/solution interface, while V_f is the potential affecting the charge migration process across the barrier oxide. Neither Meyer [36] nor MacDonald and Conway [37] speculated as to the detailed nature of the barrier film charge migration processes, since, as will be shown in the formal analysis, this point is in principle, unimportant with regard to the kinetics of oxygen evolution. It is however assumed that the rate of the field dependent migration of the charge carriers (magnitude of charge = ze) can be described by the Mott-Cabrera model [44] i.e. –

$$i = K \exp\left[\frac{ze\delta\Phi}{RT}\right] \tag{10}$$

where, i, is the current through the film, δ is the half jump distance of the charge carriers, and Φ is the magnitude of the electric field and K denotes a constant. Rewriting equation (10) in terms of the potential V_f, yields,

$$i_f = K \exp\left[\frac{ze\delta V_f}{LRT}\right] = K \exp\left[\frac{ze\beta_f V_f}{RT}\right] \tag{11}$$

where, L is the thickness of the barrier film, and $\beta_f = \delta/L$ is the symmetry factor for the field assisted migration of the charge carriers in the film. The expression for the flux or rate f_s of the interfacial electrochemical charge transfer reaction takes the standard form, i.e.,

$$f_s = k_s^{'0} \prod_i a_{i,s}^{m_{i,s}} \exp\left[\frac{\beta_s F V_s}{RT}\right] \tag{12}$$

where, $\prod_i \left(a_{is}^{m_{i,s}}\right)$ is the product of the activities of the reactants raised to the appropriate power m_i and β_s, is the symmetry factor for the reaction. For mathematical convenience, equation (11) is rewritten in the same form as (12):

$$f_f = k_f^{'0} \prod_j a_{j,f}^{m_{j,f}} \exp\left[\frac{\beta_f F V_f}{RT}\right] \tag{13}$$

Meyer [36] commented that an equation such as (13), should be regarded purely as a formal expression giving the rate of charge transport through an oxide film of constant thickness, as a function of the activities $\left(a_{jf}^{p_{j,f}}\right)$ and the potential V_f. The activities in equation (13) depend on the nature of the oxide charge migration process and may be thought of, in terms of the effective concentration of the barrier oxide film charge carriers. When the interfacial electrochemical charge transfer process (oxygen evolution in the present case) is occurring at a steady state, the rate detemining step (RDS) of that process must be in equilibrium with the charge transfer process through the film. Therefore, equating equations (12) and (13), and eliminating the V_f and V_s terms by recalling that the overall applied potential, E, is equal to the sum of these two potential terms, we achieve, after some rather laborious algebra, the following expression for the net steady state electron transfer rate f_Σ,

$$f_\Sigma = k_\Sigma \left\{\prod_i \left(a_{i,s}{}^{m_{i,s}}\right)^{\frac{\beta_f}{\beta_s+\beta_f}}\right\}\left\{\prod_j \left(a_{j,f}{}^{m_{j,f}}\right)^{\frac{\beta_s}{\beta_s+\beta_f}}\right\} \exp\left[\frac{\beta_\Sigma FE}{RT}\right] \tag{14}$$

Where

$$\beta_\Sigma = \frac{\beta_s \beta_f}{\beta_s + \beta_f} \tag{15}$$

And

$$k_{\Sigma} = k_f^{'0\frac{\beta_s}{\beta_s+\beta_f}} k_s^{'0\frac{\beta_f}{\beta_s+\beta_f}} \tag{16}$$

The term β_{Σ} as defined in equation (15) is an *overall symmetry factor* taking account of the two charge transfer barriers.

It was shown by MacDonald and Conway [37] that for a particular OER pathway (with a particular step chosen as rate controlling), the conventional kinetic analysis of which yielded a prediction of $b = 2.303(2RT/3F)$, application of the dual barrier model changed this prediction to $b = 2.303(4RT/5F)$. In our previous article [1] on the OER at Ni anodes, a reaction scheme was proposed that gave satisfactory account for the experimental observation of $b = 2.303(2RT/3F)$ and $m_{OH^-} =\sim 1$ at lower overpotentials. An analogous pathway for passive oxide covered Co anodes in aqueous alkaline solution could be written as follows:

$$\left[Co(IV)O_m(OH)_n\right]^{p-} + OH^- \rightarrow \left[Co(IV)O_m(OH)_{n+1}\right]^{p-} + e^- \tag{B I}$$

$$\left[Co(IV)O_m(OH)_{n+1}\right]^{p-} \rightarrow \left[Co(IV)O_m(OH)_{n-1}\right]^{(p-1)-} - H_2O_2 + e^- \tag{B II}$$

$$\left[Co(IV)O_m(OH)_{n-1}\right]^{(p-1)-} - H_2O_2 + 2OH^- \rightarrow \left[Co(IV)O_m(OH)_n\right]^{p-} - HO_2 + H_2O + e^- \tag{B III}$$

$$\left[Co(IV)O_m(OH)_n\right]^{p-} - HO_2 + OH^- \rightarrow \left[Co(IV)O_m(OH)_n\right]^{p-} + O_2(g) + H_2O + e^- \tag{B IV}$$

The details of this somewhat novel pathway were discussed in the first part of this series [1]. In contrast to the Ni(III) catalytic centre envisaged for Ni, the active site on oxidised Co electrode surfaces is likely to be tetravalent as discussed above (Fig. 3). The concept of *complex anionic surface species*, formed by the coordination of extra hydroxide ions facilitated by the acidic properties of hydrous oxides at significant anodic potentials in solutions of high pH, was discussed elsewhere [1, 21, 45, 46] and is retained here. As was discussed in our review of the electrochemistry of Co electrodes in aqueous alkaline solution, it is to be expected that the outer regions (where reside the reaction sites for the OER) of the passive oxide should be dispersed and hydrous in nature and it is therefore reasonable (after O'Sullivan and Burke [45]) to represent the OER catalytic entities as $[Co(IV)O_m(OH)_n]^{p-}$, where p=2m+n-4.

We now examine, whether pathway (B) can, with the adoption of the dual barrier model, account for the experimental kinetic parameters observed for the "type" C Co electrode ($b \cong 2.303(4RT/5F)$ and $m_{OH^-} =\sim 1$). We have previously outlined [1] a conventional kinetic analysis of this type of OER pathway where the second step was considered to be the rate determining step (RDS). In that analysis it was shown, that at lower overpotentials with the Langmuir isotherm assumed, the fractional coverage, θ, of the only reaction intermediate to achieve any significant coverage ($[Co(IV)O_m(OH)_{n+1}]^{p-}$ in the present case), can be written as:

$$\theta = Ka_{OH} \exp\left[\frac{FE}{RT}\right] \tag{17}$$

In equation (17) $K = k_1^{'0}/k_{-1}^{'0} = \exp\left[-\Delta G^{'0}/RT\right]$, where $k_1^{'0}, k_{-1}^{'0}$ are respectively, the standard electrochemical rate constants for the initial discharge step in the forward and reverse directions. Under the dual barrier model, with step (B II) taken as rate limiting, the rate equation for the interfacial OER (expressed now in terms of its current density i_s-c.f.eqn.12) becomes [c]:

$$\begin{aligned} i_s &= 2Fk_2^{'0}\theta\theta_{sc}\exp\left[\frac{\beta_s FV_s}{RT}\right] \\ &= 2Fk_2^{'0}K\theta_{sc}\exp\left[\frac{FE}{RT}\right]a_{OH}\exp\left[\frac{\beta_s FV_s}{RT}\right] \end{aligned} \tag{18}$$

Equating the expressions outlined in eqn. 18 and eqn.13, and eliminating, as before, the V_f and V_s terms, yields the following expression for the overall current density (through the two barriers),

$$i = 2FK_\Sigma^{'}\theta_{sc}\left(a_{OH}\right)^{\frac{\beta_f}{\beta_s+\beta_f}}\exp\left[\frac{\left(1+\beta_\Sigma\right)FE}{RT}\right] \tag{19}$$

Where we note that $K_\Sigma^{'} = k_2^{'0}KK_\Sigma\left\{\prod_j\left(a_{j,f}^{m_{j,f}}\right)^{\frac{\beta_s}{\beta_s+\beta_f}}\right\}$.

Assuming that both barriers are symmetrical (i.e. $\beta_f = \beta_s = ½$) and inserting these values into equation (15), gives $\beta_\Sigma = 1/4$. Inserting this value for the overall symmetry factor into equation (19) yields:

$$i = 2FK_\Sigma^{'}\theta_{sc}a_{OH}^{1/2}\exp\left[\frac{5FE}{4RT}\right] \tag{20}$$

The predicted values for b and m_{OH}, are thus:

$$\begin{aligned} b &= \left(\frac{\partial E}{\partial\log i}\right)_{a_{OH}} = 2.303\left(\frac{4RT}{5F}\right) \\ m_{OH} &= \left(\frac{\partial\log i}{\partial\log a_{OH}}\right)_E = \frac{1}{2} \end{aligned} \tag{21}$$

It is clear that while, application of the dual barrier model to the oxygen evolution pathway of scheme (B) (with (B II) as RDS and $\theta \rightarrow 0$), leads to the prediction of the experimentally observed Tafel slope for "type" C Co electrodes, it cannot account for the observed reaction order of approximately unity. Reaction order considerations were not treated in the original paper of MacDonald and Conway [37], however it is obvious from equation (14) that the *apparent reaction order* with respect to the activity a_s of a particular reactant species in the electrochemical charge transfer reaction, as measured by $(\partial\log i/\partial\log a_s)_E$ is given by the expression:

$$\left(\frac{\partial\log i}{\partial\log a_s}\right)_E = \frac{m_s\beta_f}{\beta_s+\beta_f} \tag{22}$$

That is to say, that in cases where a potential dependent, field driven charge migration process occurs in series with the interfacial charge transfer reaction, the experimentally measured $(\partial \log i/\partial \log a_s)_E$ quantity is actually a fraction, $\beta_f/\beta_f+\beta_s$, of the true reaction order m_s for the latter reaction. If it is again assumed that $\beta_f = \beta_s = ½$, then the quantity $\beta_f/\beta_f+\beta_s = ½$. This explains why the kinetic analysis of scheme (B) under dual barrier conditions, yielded a value of $(\partial \log i/\partial \log a_{OH})_E = ½$, rather than the order of unity that is derived [1] in the conventional (single barrier) analysis of such a pathway.

From the point of view of our experimental data, if we admit the applicability of the dual barrier model (assuming again that $\beta_f = \beta_s = ½$ and thus, $\beta_f/\beta_f+\beta_s = ½$), the observation of an experimental apparent reaction of ~1 in association with a lower overpotential Tafel slope of ~2.303×4RT/5F, implies that the analysis of an appropriate pathway for the OER on "type" C Co electrodes must predict b = 2.303×2RT/3F and a reaction order of *two*, when the oxygen evolution reaction is considered in isolation from the oxide film charge transfer process. It should be clear, that this would arise if there was a additional factor of a_{OH} in rate equation (18) – in other words in a suitable reaction pathway, as well as the mole discharged in the initial step, a further mole of OH^- ions are adsorbed from the bulk solution, per mole of active surface sites, in the RDS, or in another step that occurs between the initial step and the RDS. Furthermore, to account for the low Tafel slope of 2.303×2RT/3F, the RDS must be an electrochemical rather than chemical reaction.

It can be shown [35] that several previously proposed pathways, satisfy the criteria outlined above. These include the Krasil'shchikov pathway (A), if step (A III) is considered to be rate-controlling (with $\theta_{SO^-} \rightarrow 0$) and the Bockris Electrochemical path [35] again with the second electron transfer step taken as the RDS and low coverage Langmuir adsorption conditions assumed. Indeed, on the sole basis of the experimental kinetic data of Figs. 6 and 7, it is impossible to further discriminate between several possible OER pathways.

3.9. A consistent mechanism for all ' types' of Co electrodes

In an attempt to advance the problem of mechanistic determination beyond the deadlock outlined in the previous paragraph, we turn to the experimental kinetic parameters obtained for the "type" B electrode: b = ~60 $mVdec^{-1}$, m_{OH^-} = ~3/2 at lower η, and b = ~120 $mVdec^{-1}$, m_{OH^-} = ~1 at higher η. These results are identical to those that we have reported elsewhere [21] for the OER at multicycled and aged Fe anodes. The only pathway that we could identify to suitably account for the aforementioned set of kinetic parameters, was of the following general form,

$$S + OH^- \rightarrow S - OH + e^- \quad \text{(CI)}$$

$$S - OH + OH^- \rightarrow S - H_2O_2 + e^- \quad \text{(C II)}$$

$$S - H_2O_2 + OH^- \rightarrow S - HO_2^- + H_2O \quad \text{(C III)}$$

$$S - H_2O_2 + S - HO_2^- \rightarrow O_2(g) + H_2O + OH^- \quad \text{(C IV)}$$

where, as before, S is a catalytically active surface site and $-H_2O_2$ represents *physisorbed* hydrogen peroxide. If step (C II) is taken as the RDS, it can be shown [21] that for high fractional coverage of S-

OH (Langmuir isotherm, $\theta_{S\text{-}OH} \rightarrow 1$), a conventional kinetic analysis predicts $b = 2.303\left(2RT/F\right)$ (118.3 mVdec^{-1} at 25ºC) with $m_{OH^-} = 1$. On the other hand, over the potential window where an intermediate coverage of S-OH prevails (Temkin isotherm, $0.2 \leq \theta_{S\text{-}OH} \leq 0.8$), values of $b = 2.303\left(RT/F\right)$ (59.2 mVdec^{-1} at 25ºC) and $m_{OH^-} = 3/2$ are predicted. The reason behind the requirement for a physisorbed, as opposed to chemisorbed, product in step (C II) was also discussed in that article [21]. Pathway (C) was originally devised by Bockris and Otagawa [35], for the OER on cobaltate and ferrite electrodes in alkaline solution.

Consider the form of the overall rate equation for scheme (C), if again the second step is rate limiting, but on this occasion the fractional coverage of S-OH is considered to follow the Langmuir isotherm at lower overpotentials. If the quasi-equilibrium principle is applied to step (C I), it is clear that the fractional coverage of S-OH is again given by equation (17). The overall OER current density, *i*, is then given by:

$$\begin{aligned} i &= 2Fk_2^{'0}a_{OH}\theta \exp\left[\frac{\beta F\eta}{RT}\right] \\ &= 2Fk_2^{'0}Ka_{OH}^2 \exp\left[\frac{(1+\beta)F\eta}{RT}\right] \end{aligned} \tag{23}$$

Assuming that $\beta = ½$ we can readily show that eqn.23 yields the following expressions for *b* and m_{OH}:

$$\begin{aligned} b &= \left(\frac{\partial\eta}{\partial\log i}\right)_{a_{OH}} = 2.303\left(\frac{2RT}{3F}\right) \\ m_{OH} &= \left(\frac{\partial\log i}{\partial\log a_{OH}}\right)_{\eta} = 2 \end{aligned} \tag{24}$$

As discussed in the previous section, where a conventional (single barrier) electrode kinetic analysis gives rise to these values for *b* and m_{OH}, a treatment under the dual barrier model would lead to $b = 2.303\left(4RT/5F\right)$ and $m_{OH} = 1$.

Notwithstanding the fact that physisorbed species are classically considered to have greater surface mobility relative to chemisorbed entities, it is somewhat difficult to envisage how the recombination step (C IV) could proceed at a sufficient velocity under low coverage Langmuir conditions, such as not to render it rate-determining overall. We therefore present the following modification to the original physisorbed peroxide pathway of Bockris and Otagawa, which avoids the latter difficulty:

$$\left[Co(IV)O_m(OH)_n\right]^{p-} + OH^- \rightarrow \left[Co(IV)O_m(OH)_{n+1}\right]^{p-} + e^- \quad \text{(D I)}$$

$$\left[Co(IV)O_m(OH)_{n+1}\right]^{p-} + OH^- \rightarrow \left[Co(IV)O_m(OH)_n - H_2O_2\right]^{p-} + e^- \quad \text{(D II)}$$

$$\left[Co(IV)O_m(OH)_n - H_2O_2\right]^{p-} + OH^- \rightarrow \left[Co(IV)O_m(OH)_n - HO_2\right]^{p-} + H_2O + e^- \quad \text{(D III)}$$

$$\left[Co(IV)O_m(OH)_n - HO_2\right]^{p-} + OH^- \rightarrow \left[Co(IV)O_m(OH)_n\right]^{p-} + O_2(g) + H_2O + e^- \quad \text{(D IV)}$$

As we commented elsewhere [1], the extreme irreversibility of the oxygen evolution and reduction reactions prevents the accurate and meaningful evaluation of the stoichiometric number, v, thus removing the possibility of experimental discrimination between pathway (C) ($v = 2$ with (C II) as RDS) and pathway (D) ($v = 1$ with (D II) as RDS).

It is obvious that the formal kinetic analysis of scheme (D), with the second step rate-determining under low coverage Langmuir adsorption conditions, is identical to that considered in equations (23) and (24). This means, of course, that (D) is yet another mechanism that can account for the experimental kinetic parameters observed for the "type" C Co electrode. However, exclusively amongst the candidate mechanisms, the physisorbed peroxide pathway of (C) or (D) can also rationalise the steady state polarisation data obtained for the "type" B Co anode, as was discussed earlier in the present section. On this basis we would suggest that (D) *is the most likely reaction pathway* for the OER on passive oxide covered Co electrodes in aqueous alkaline solution. Attributing the changes, with electrode ageing, in the experimental values of the diagnostic parameters, to changes in intermediate adsorption conditions, while maintaining a consistent reaction pathway, would seem to provide a more coherant solution than envisaging entirely different mechanisms for the "type" B and C anodes, considering that both are fundamentally passivated Co electrodes. Furthermore, the same pathway and adsorption conditions are likely for the "type" A Co electrode (fresh non-pre-treated) as the "type" C anode (fresh pre-reduced). The slope of $b \approx 2.303(4RT/5F)$ observed for the "type" A electrode in 1.0 M NaOH is similar to that which characterises the "type" C electrode at all electrolyte concentrations. The lower slope of $b \approx 2.303(2RT/3F)$ recorded for the "type" A electrode in 5.0 M NaOH is characteristic of pathway D proceeding without a series oxide layer potential barrier – the reason for the applicability of the dual barrier model to this type of electrode in 1.0 M NaOH but not in 5.0 M NaOH will be discussed in the next section. For the moment it is noted that a change in the operative adsorption isotherm at lower overpotentials, from the low coverage Langmuir isotherm for the "type" A electrode, to the Temkin isotherm for the "type" B electrode, would certainly appear to be consistent with the comparitive polarisation plots presented in Fig. 8.

The question arises as to why the concentration of the adsorbed intermediate $[Co(IV)O_m(OH)_{n+1}]^{p-}$, is greater over the range of potentials associated with the lower linear Tafel region, for the aged ("type" B) Co electrode relative to the fresher electrodes ("types" A and C) of the same metal. On the basis of the voltammetric profile of the "type" B electrode (Fig. 9), with its unusually large background charge, we speculate that a more hydrous and dispersed oxide phase forms on this electrode surface compared to that of the fresher anodes. We commented previously, this probably arises as a cumulative result of a continuous cycle, over a long period of service, of mechanical polishing (which we have shown to be not completely effective in the removal of oxide phases) and subsequent re-passivation of surfaces containing some residual oxide material. It may also be related to the long term ageing of a thin residual oxide phase, adjacent to the metal, which is particularly resistant to removal by polishing.

As discussed elsewhere [21], the amphotheric nature of electrochemically generated phase oxides becomes more prevalent with increasing degrees of hydration and dispersion. On this basis, it is to be expected that the aged "type" B electrode would contain a relatively larger surface density of the

catalytically active, complex anionic $[Co(IV)O_m(OH)_n]^{p-}$ species at lower oxygen evolution overpotentials, in comparison to the fresher electrodes. The polarisation data of Fig. 9 indicates that as η is increased, the concentration of the surface catalytic centres on the fresher electrode effectively "catches up" with that of the aged electrode, and consequently the oxygen evolution current densities for both electrodes become convergent at higher overpotentials.

Returning momentarily to the dual barrier model, some further evidence for its applicability in the rationalisation of the OER steady state polarisation behaviour of "type" C Co electrodes, can be obtained by considering the situation at higher overpotentials. The approximation that gave rise to equation (17) is no longer applicable, and it is necessary to return to the full expression (that we have derived elsewhere [1]) for θ:

$$\theta = \frac{Ka_{OH}\exp\left[\frac{FE}{RT}\right]}{1+Ka_{OH}\exp\left[\frac{FE}{RT}\right]} \tag{25}$$

For sufficiently high E, the $Ka_{OH}e^{EF/RT}$ term becomes very much larger than unity, and therefore θ approaches unity. By analogy with equations (18) and (23), the rate equation for the OER proceeding via pathway (D) (step (D II) as RDS), under dual barrier conditions is given by:

$$i_s = 2Fk_2^{'0}\theta a_{OH}\exp\left[\frac{\beta_s FV_s}{RT}\right] \tag{26}$$

In the limit of $\theta \rightarrow 1$, the expression for the overall current through both barriers becomes,

$$i = 2FK_{\Sigma}^{"}\left(a_{OH}\right)^{\frac{\beta_f}{\beta_s+\beta_f}}\exp\left[\frac{\beta_{\Sigma}FE}{RT}\right] \tag{27}$$

where we note that $K_{\Sigma}^{"} = K_{\Sigma}^{'}/K$.

If, as before, it is assumed that $\beta_f = \beta_s = ½$, and logarithms are taken of each side of equation (27), it follows that:

$$\begin{aligned} b &= \left(\frac{\partial E}{\partial \log i}\right)_{a_{OH}} = 2.303\left(\frac{4RT}{F}\right) \\ m_{OH} &= \left(\frac{\partial \log i}{\partial \log a_{OH}}\right)_E = \frac{1}{2} \end{aligned} \tag{28}$$

No systematic attempt was made to determine Tafel slopes and associated reaction orders at higher overpotentials for "type" C electrodes, owing to the presence of an unusual "local maximum" feature at potentials spanning the approximate range of 0.75 – 0.85 V, in the log i vs. E characteristics of Fig. 6. Nevertheless, at potentials anodic to this feature, the polarisation plots (at least for 1.0 M

≤[OH^-]≤ 5.0 M) are resolved into a linear region with a slope of $b \approx 2.303\left(\frac{4RT}{F}\right)$ (~236 $mVdec^{-1}$ at 25ºC). While further, specifically targeted experimentation is required, to obtain a more complete understanding of this region of the polarisation plot (for example the origin of the "maximum" feature), it is worth commenting, with reference to the analysis of equations (25) – (28), that the observation of log *i* vs. *E* slopes of $b \approx 2.303\left(\frac{4RT}{F}\right)$ is consistent with our proposed reaction pathway, (D), proceeding with $\theta \rightarrow 1$, under dual barrier conditions. A summary is provided in Table 2 of the various values of the experimental kinetic parmeters (*b* and associated m_{OH}) that we have observed for the OER at oxidised Co electrodes and the conditions under which they can be rationalised by pathway (D).

Table 2. Summary of the various experimentally observed kinetic parameters, and the conditions under which they can be rationalised by pathway D.

Co Electrode type	Experimental b, m_{OH}	Dual Barrier ?	b, m_{OH} for analysis	Adsorption Isotherm
A	$2RT/3F$ (5M) $\rightarrow 4RT/5F$ (1M)	lower [OH^-]	----	----
B, low η	RT/F, 3/2	No	As listed left	Temkin, $r_I >> r_{II}$ [a]
B, upper η	$2RT/F$, 1	No	As listed left	Langmuir, $\theta \rightarrow 1$
C, low η	$4RT/5F$, 1	Yes	$2RT/3F$, 2	Langmuir, $\theta \rightarrow 0$
C, upper η	$4RT/F$	Yes	$2RT/F$	Langmuir, $\theta \rightarrow 1$

[a] r_I , r_{II} are the Temkin parameters for the intermediates formed in the first and second steps respectively. See reference 21 for more details.

3.10. The physical origin of the oxide layer charge transfer barrier

The most pressing outstanding issue, relates to the polarisation curves of Fig. 5, recorded for a "type" A Co electrode in solutions with different OH^- ion concentrations. Specifically, it might be asked, why there is an oxide film charge transport barrier in series with the interfacial electrochemical charge transfer barrier in the case of the data recorded in 1.0 M NaOH solution (giving rise to $b \approx 2.303(4RT/5F)$, but not for the polarisation curve recorded in 5.0 M NaOH solution ($b \approx 2.303(2RT/3F)$?

It is our view, that the key to answering this question lies in the identification of the oxide film charge transfer barrier with the inner inner compact anhydrous region of the anodic oxide films, or with the interface between this inner region, and the outer more disperse and hydrated region of these films. Recall from our review of the surface electrochemistry of Co electrodes, that passivation is generally accepted to occur, initially by the formation of a Co(II) based oxide on the metallic surface, the outer regions of which are then further oxidised to hydrous higher oxides (sandwich model). In the general model of this type of passive oxide, developed by Burke and co-workers [18, 19] and discussed by us elsewhere [21], it is envisaged that the majority of the potential drop across the oxide film occurs at the compact layer/dispersed layer interface. According to this model, under conventional steady state anodization conditions, the inner compact layer is likely to be of limited thickness since the activation energy for atom or ion migration is generally quite large. This is due to the fact that in this amorphous, anhydrous inner layer, the ions are held in a rigid manner, in a network of polar covalent bonds that drastically reduce ion transport through this region of the oxide, in turn inhibiting its expansion. In contrast, the model envisages that the outer more dispersed region of the oxide has a similar morphology to redox polymers with transfer of electrons along the "polymer" chains via a process of self exchange between neighbouring oxy metal groups [21]. In terms of this dual layer model, it would certainly seem that the inner anhydrous oxide region fits the profile of the barrier oxide envisaged by Meyer [36], and MacDonald and Conway [37].

Earlier, it was concluded, with reference to the voltammetric data of Figs. 1 and 2, that in solutions of lower OH^- ion concentration, the initial passivation of the electrode occurs essentially via a *solid state* Co→Co(II) oxidation process. With increasing concentration, especially for $[OH^-] > 1M$, a rapid *dissolution/precipitation* mechanism becomes progressively more important in the formation of the initial Co(II) oxyhydroxide film. The oxide formed primarily by the solid state route is expected to be a compact structure based on polar covalent bonding – in fact just the type of oxide that we have proposed to form a significant barrier to charge transfer. It is therefore not surprising that the dual barrier model is apparently applicable to the kinetics of the OER at bright Co electrodes in solutions where $[OH^-] \leq 1$ M.

On the other hand, the oxide film formed by a rapid dissolution/precipitation reaction, is lightly to be a somewhat crystalline phase albeit with a high defect concentration, owing to the rapid rate of re-precipitation, as envisaged by Erts et al. [23]. Such a phase, would be expected to be characterised, by significantly higher electronic conductivity and ionic mobility, than the inner oxide region formed at lower $[OH^-]$, and thus present a much lower potential barrier to charge migration. The aforementioned considerations provide a satisfactory explanation for the appearance of dual barrier Tafel slope behaviour in the 1.0 M steady state polarisation curves of Fig. 5, while such behaviour is absent from the data recorded in 5.0 M NaOH solutions.

In the case of "type" C Co electrodes (Fig. 6), for which a reproducible Tafel slope of $b \approx 2.303(4RT/5F)$ (with an associated reaction order of approximately unity) was noted over a range of OH^- concentrations, the applicability of the dual barrier model at all concentrations can be attributed to the pre-treatment regime. Recall that these electrodes were pre-reduced at –1.15 V in 1 M NaOH for five minutes. Polarisation at such a low cathodic potential should be effective in rupturing the polar covalent bonds between metal cations and oxyanions, and therefore weakening, if not completely

reducing any residual compact oxide structures (resistant to removal by polishing) remaining from previous experiments. As outlined in the "Experimental" section, the electrodes were subjected, following the pre-reduction, to a voltammetric cycle in the same 1.0 M NaOH. This meant that the initial re-passivation of the electrode occurred under identical conditions prior to each OER polarisation experiment. Therefore the nature of the innermost compact oxide, adjacent to the metal surface, could be expected to be relatively independent of the concentration of the test solution in which the electrode was to be polarised. By pre-treating the electrodes in 1.0 M NaOH solution, a barrier type inner compact oxide was formed prior to each polarisation measurement, thus removing the variable that caused a change in Tafel slope with OH^- concentration, and allowing an accurate determination of the reaction order m_{OH}, subject to the correction required under the dual barrier model.

Further justification of our identification of the oxide charge migration barrier, with the inner compact region of the passive film formed on certain transition metals, can be found by looking beyond our own work. For example, O'Sullivan and Burke [45] prepared thick hydrous oxide films on Rh electrodes in 1.0 M NaOH, by repetitive potential cycling at a rapid rate of ca. $6Vs^{-1}$ between the limits of 0 and 1.50 V (vs. R.H.E.) for the duration of 3600 cycles. Oxygen evolution steady state polarisation measurements conducted directly on this pre-cycled electrode, indicated a lower Tafel slope of ca. 48 $mVdec^{-1}$. In a separate experiment, these workers, subjected an electrode, pre-cycled exactly as before, to a further 255 potential cycles at a much slower rate of 195 mVs^{-1} between extended limits of 0 – 1.9 V, before conducting the steady state polarisation measurement. On this occasion a Tafel slope of ca. 40 $mVdec^{-1}$ was observed. This might be explained by the fact, that during the excursions to cathodic potentials on the slower sweeps (195 mVs^{-1}), sufficient time was available to affect a significant reduction of the inner region of the oxide film, effectively removing the barrier layer that might well have been the cause of the higher Tafel slope observed in the other experiment.

3.11. Estimation of electrode roughness factors

As discussed in the first part of this series [1], there is a scarcity of suitable techniques for the evaluation of the electrode roughness factor, f_r, for passive oxide covered Ni, Co or Fe anodes. In the case of Ni, we adopted an electrode charge/discharge technique (the OH_{ads} desorption method) originally described by Ho and Piron [6]and the same approach was followed for the Co anodes.

The method involves the galvanostatic charging of the working electrode at a number of current densities, i_{appl}, corresponding to the OER proceeding in the steady state at known overpotentials η. The electrode is then discharged to ground through a 1Ω series resistor, with the cathodic decay current–time (*i-t*) transient recorded by a digital storage oscilloscope connected across the resistor. Integration of this transient between the instant of the interruption of charging and the time at which the decay current became zero, yields a value for the total charge, Q_{dec}, passed in the course of the discharge process. It is envisaged that the discharge of the electrode occurs by the desorption of the intermediate species involved in oxygen evolution. An overall discharge reaction

consistent with our favoured OER pathway for Co anodes (i.e. (D)) can therefore be written as:

$$\left[Co(IV)O_m(OH)_{n+1}\right]^{p-} + H_2O + 2e^- \rightarrow \left[Co(III)O_{m-1}(OH)_{n+1}\right]^{p-} + 2OH^- \quad (29)$$

As is evident from Fig. 16, plots of Q_{dec} vs. η are characterised by a steady increase in Q_{dec} with increasing η for lower values of the latter. At higher overpotentials a plateau is reached where relatively constant values of Q_{dec} are observed over a range of overpotentials. It was proposed by Ho and Piron[6] that the plateau in such Q_{dec} vs. η plots, corresponds to the desorption of the electrosorbed intermediate (OH_{ads}) for the situation where the coverage of this species approaches a full monolayer. As we explained in more detail in the first part of this series[1], for a two electron desorption (as in (30)), it is envisaged that a reasonable *estimate* of the electrode roughness factor is provided by the expression:

$$f_r = \frac{Q_{dec}\,(plateau)}{420\,\mu C\,cm^{-2}} \quad (30)$$

Regarding reaction (29), it is proposed that desorption of the OER intermediate, results in the reduction of the ions of the oxide surface to the +3 cobalt oxidation state. Referring to the CV of Fig. 1, it is obvious that the voltammetric features generally attributed to the oxidation of Co^{2+} to Co^{3+} species have their onset potentials in the range of 0 – 0.1 V – i.e. significantly lower than the oxygen electrode reversible potential(0.303 V). This observation suggests that discharge of the surface Co ions of the anodic oxide film should continue to the Co(III) oxidation state, following the interruption of a steady state polarising current corresponding to a significant rate of the OER. This viewpoint is also supported by thermodynamic data[9] which indicates that the oxidation of Co(II) species should begin in the region of –0.4 V (vs. Hg/HgO, 1M KOH), with Co_3O_4 being the initial oxidation product.

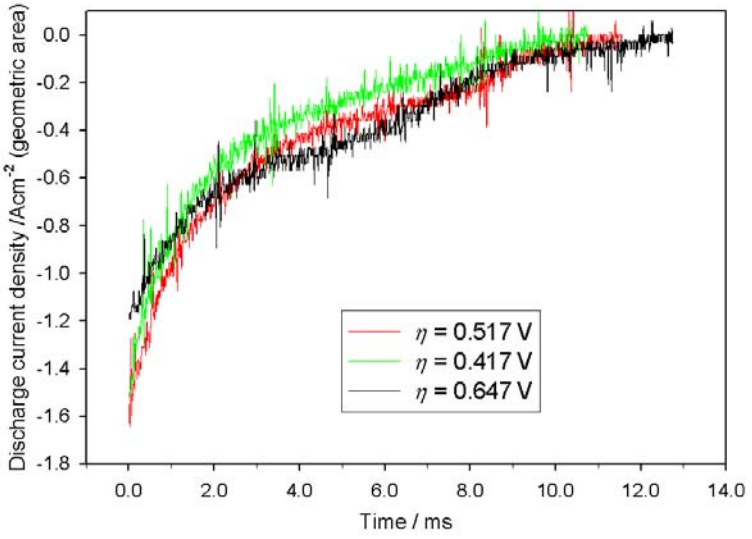

Figure 15. Raw decay current transients for a "type" C Co electrode in 1.0 M NaOH solution. Indicated are the overpotentials corresponding to the values of i_{appl} in each case.

Typical raw discharge current decay transients are presented in Fig. 15 for a "type" C Co electrode in 1.0 M NaOH solution, following the interruption of prior anodic charging current densities corresponding to the overpotentials indicated in the legend. The overall results of the current decay experiments for this system are presented in the form of a Q_{dec} vs. η plot in Fig. 16. The close relationship between the Q_{dec} vs. η plot and the steady state polarisation curve for a given system, as discussed in more detail elsewhere[1, 6], is illustrated in Fig. 16 by the inclusion of the log$i(\eta)$ characteristic for the same "type" C electrode, also in 1.0 M NaOH. Also included is $Q_{dec}(\eta)$ data for a "type" A Co anode in 1.0 M NaOH solution – for clarity the steady state polarisation plot for this system is omitted. The $Q_{dec}(\eta)$ data points represent the mean value of Q_{dec} calculated from four transients, recorded in separate experiments, for each value of i_{appl}, while the vertical error bars span ± one standard deviation from this mean.

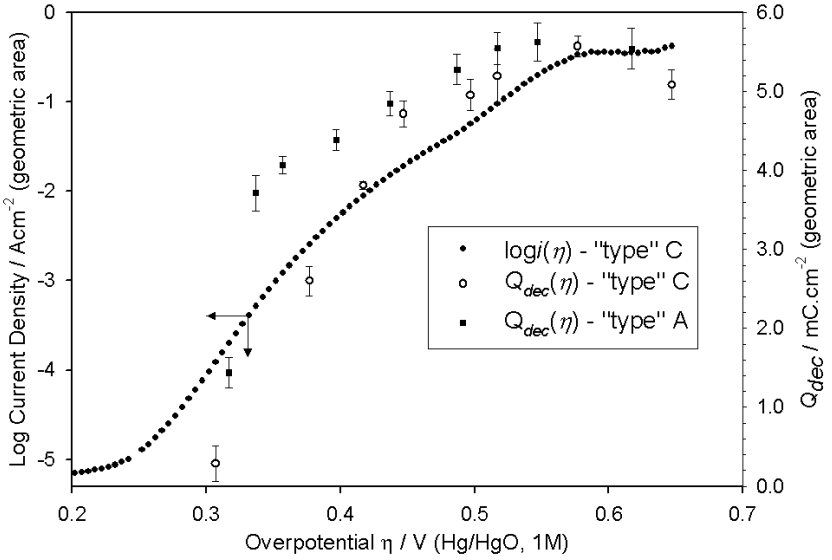

Figure 16. Total charge, Q_{dec}, passed during the discharge of "types" A and C Co electrodes in 1.0 M NaOH vs. oxygen evolution overpotential η. Also included is the steady state polarisation curve for the "type" C electrode.

Applying a similar approach, to that which we outlined previously [1], for extracting the most appropriate value for Q_{dec}(plateau) from the raw data of Fig. 16, values of f_r were calculated for both electrodes. The results are tabulated in Table 3. As in our previous article [1], it is emphasised that the quoted error refers simply to the experimental error – the true error is likely to be significantly greater, owing to the questionable nature of some of the assumptions on which the technique is based [6].

Referring to the EIS data of Figs. 12 and 13, and the optimised values of the equivalent circuit elements listed in Table 1, it is apparent that the measured values of the double layer capacitance, C_{dl}, for the "type" C electrode in 1.0 M NaOH, decrease steadily with increasing η. Such behaviour was also noted for oxidised Ni anodes, and was explained in terms of a decrease in the average "wettable" electrode surface area, caused by increasingly vigourous oxygen bubble formation as the overpotential is increased[1]. It was therefore suggested that the most appropriate fitted value of C_{dl} to use for the

estimation of f_r, by the well known *double layer capacitance ratio method* [47], would be that obtained from EIS data recorded at overpotentials just above the onset potential for significant OER current densities. This approach was successfully applied to roughness factor estimation for a *pre-reduced* Ni electrode, however it proved unsuitable in the case of a *pre-oxidised* Ni anode, owing to the relatively low value (α = 0.802) of the fitted, double layer, CPE α parameter (see equation (8)) in the latter case[1]. Such a low α value, implies that the double-layer impedance response is not strongly identifiable with the classical concept of a capacitance, and it was concluded that performing a capacitance ratio analysis would lead to a dubious estimation of f_r. From Table 1, it is obvious that the situation is not much better for the "type" C Co electrode, with fitted paramters of $0.807 \leq \alpha \leq 0.825$ noted for lower OER overpotentials. It must therefore be concluded, that the EIS data recorded for the "type" C Co anode, does not facilitate the useful estimation of the electrode active surface area by the double layer capacitance ratio method.

Table 3. Summary of the roughness factors, f_r, determined for the "type" A and C Co electrodes in 1.0 M NaOH solution, using the OH_{ads} desorption method.

Co Electrode type	Q_{dec} (plateau) mC/cm^2	f_r
A	5.5 ± 0.2	13.1 ± 0.5
C	5.4 ± 0.3	12.9 ± 0.7

3.12. Comparison of the intrinsic activities for the OER of the differently pre-treated Co electrodes

Steady state polarisation curves for "type" A and C Co electrodes in 1.0 M NaOH solution, with the log *i* values normalised according to the roughness factors of Table 3, are presented in Fig. 17. Clearly, compared to the pre-reduced "type" C electrode, the non-pre-treated "type" A anode exhibits a somewhat greater catalytic activity towards oxygen evolution over the approximate range of $0.26V \leq \eta \leq 0.5V$. This is apparently related to the marginally larger Tafel slope (b = 47.5 mVdec^{-1}) observed for the former, relative to the latter(b = 46.0 mVdec^{-1}). In our kinetic analysis of pathway (D), proceeding under dual barrier conditions with the second step as RDS and low intermediate species coverage sssumed, it was shown that at 25°C a value of $b = 2.303(4RT/5F)$ = 47.3 mVdec^{-1} is predicted. If it assumed that the potential barrier for the interfacial electron transfer process is symmetrical (i.e. β_s = ½), then the slight numerical differences of the measured Tafel slopes from 47.3 mVdec^{-1} can be attributed to *not perfectly symmetrical barriers* for the barrier oxide film electron charge transfer process.

If this argument is persued, it is trivial to show [30] that for the "type" A anode, b = 46.0 mVdec^{-1} corresponds to β_f = 0.665, while the Tafel slope of 47.5 mVdec^{-1} recorded for the "type" C electrode, corresponds to β_f = 0.482 - an almost perfectly symmetrical barrier. As noted in relation to equation (11), $\beta_f = \delta/L$, implying that β_f is inversely proportional to the thickness of the barrier oxide

layer, which we have associated with the inner compact region of the passive oxide film. Following this logic, the pre-treatment routine utilised in the preparation of "type" C electrodes produces an inner passive layer of such thickness L, that it acts as almost an ideal symmetrical barrier for charge migration. In the case of the non-pre-treated "type" A Co electrode, the inner compact region of the passive layer has not developed to a sufficient thickness to provide a symmetrical energy barrier. The value of $\beta_f = 0.665$ calculated for this situation, implies that approximately 2/3 of the energy associated with the electric field across the barrier layer is available to the charge migration process, as compared to only ½ in the case of the (almost) symmetrical energy barrier that prevails in the case of the "type" C electrode. This in turn leads to a greater rate of the overall twin barrier process at a given overpotential, for the "type" A compared to the "type" B electrode.

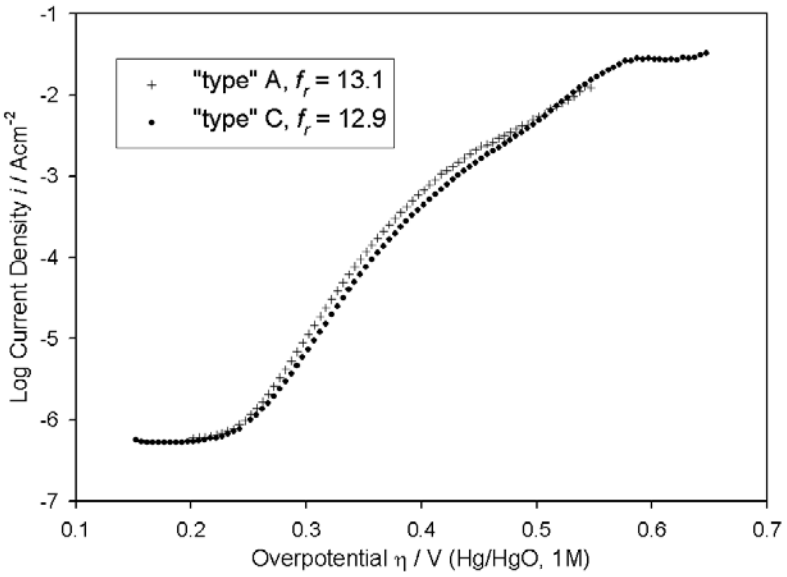

Figure 17. *iR* corrected steady state polarisation curves recorded in 1.0 M NaOH solution, for the "type" A and C Co electrodes. The values of log $i(\eta)$ are normalised to the estimated truly active surface areas, based on the stated roughness factors.

The irreproducibility of OER steady state polarisation curves recorded for Ni electrodes that were not electrochemically pre-treated, and the variation in the (active surface area normalised) OER electrocatalytic performance of Ni anodes subjected to different pre-treatment regimes, were outlined previously [1]. We interpreted these phenomena in terms of variations in the relative amounts of the active material existing in the β-β and α-γ cycles, with β-NiOOH envisaged to be the "right type" of oxide for the electrocatalysis of the OER. In contrast, the small differences in OER electocatalytic activities displayed by the Co anodes in Fig. 17 is, as discussed above, more likely to be related to differences in the charge transport properties of the underlying oxide films, than the chemical identity of the surface species. Although there apparently exist strong similarities in the hydroxide/oxyhydroxide electrochemistry of Ni and Co [48], effects of the transition of the active

material between different Bode cycles (β-β and α-γ) on the OER performance of electodes, are apparently insignificant in the case of Co by comparison with Ni. This is also bourn out by the fact, that it is possible with Co unlike Ni, to record reproducible OER polarisation data for anodes that have only been subjected to polishing and no electrochemical pre-treatment ("type" A Co electrode). In turn this may be related to the fact, that the OER catalytic sites for Co are most likely based on tetravalent metal cations, the surface density of which, at a given overpotential, will have a weaker dependence on details of the divalent-trivalent redox chemistry of the active material, than is the case with Ni, for which we have envisaged [1] Ni(III) ions to be the OER active centres.

4. CONCLUSIONS

While several of the OER pathways, previously proposed in the literature, can account for the kinetic parameters observed for a given "type" (in the context of the present work "type" refers either to a specific pre-treatment regime or the electrode age) of Co electrode, only one (pathway (D)), can coherently rationalise all the experimental data reported in the present work, for passive oxide covered Co anodes in aqueous alkaline solution. This mechanism is a more general form of the physisorbed peroxide pathway that we have previously proposed for the OER at oxidised Ni electrodes.

It has been necessary to appeal to a dual barrier model for the explanation of experimental Tafel slopes of $b \approx 2.303(4RT/5F)$, observed in particular circumstances. This dual barrier model, originally proposed by Meyer [36] and MacDonald and Conway [37], envisages that the normal potential barrier for the interfacial electron transfer reaction (OER in the present case), exists in series with another barrier, which affects the migration of charge across the oxide film under the influence of an electric field. Our development of the model, has been to identify, based on voltammetric evidence, the barrier oxide layer, with the inner compact anhydrous region of the passive oxide film, as opposed to the outer more hydrous and dispersed component.

In contrast to Ni and Fe electrodes, it was not possible, for a 1.0 M NaOH solution, to verify using ac impedance measurements, the value of *b* obtained by the normal dc steady state polarisation method. This was due to the lack of resolution, on the experimental timescale, of the total faradaic resistance at low frequencies. In turn, this arose due to an unusually large lower frequency capacitive contribution, which we have attributed to an non-homogeneous surface charge distribution associated with the Co(III)→Co(IV) redox process, in parallel with the adsorption pseudo-capacitance of the OER intermediate species.

In contrast to oxidised Ni anodes, there is no evidence for a strong variation in OER performance, related to the relative amounts of the active material in the different Bode cycles (β-β and α-γ).

ACKNOWLEDGEMENT
The authors are grateful for the financial support of Enterprise Ireland Grant Number SC/2003/0049, IRCSET Grant Number SC/2002/0169 and the HEA-PRTLI Program.

Notes and References

‡**a** Recall that the Tafel slope is related to the overall transfer coefficient, α, as follows: $b = 2.303RT/\alpha F$.
b The rather complex relationships between the frequency dependent *ac adsorption pseudocapacitance*, $\hat{C}_{ac}$, which is the quantity measured by EIS, the well known *steady state adsorption pseudocapacitance*, and the value of the equivalent circuit element $C_{ø}$, has been discussed by Harrington and Conway in reference 29.
c The θ_{sc} term represents the fractional coverage of the anionic surface complex, $[Co(IV)O_m(OH)_n]^{p-}$, and has a significance analogous to that of the θ_V term originally introduced by Bockris and Otagawa[35] for their lattice oxygen OER pathway, as was discussed in reference 1.

1. M.E.G. Lyons, M.P. Brandon, *Int. J. Electrochem. Sci.,* 3 (2008) 1386
2. H. Willems, A.G.C. Kobussen, J.H.W. De Wit and G.H.J. Broers, *J. Electroanal. Chem*, 170(1984) 227.
3. H. Willems, A.G.C. Kobussen, I.C. Vinke, J.H.W. De Wit and G.H.J. Broers, *J. Electroanal. Chem*, 194(1985) 287.
4. R.F. Scarr, *J. Electrochem. Soc.*, 116(1969) 1526.
5. L.D. Burke, M.E.G. Lyons and O.J. Murphy., *J. Electroanal. Chem*., 132(1982) 247.
6. J.C.K. Ho and D.L. Piron, *J. Appl. Electrochem.*, 26(1996) 515.
7. M.R. Gennero De Chialvo, A.C. Chialvo, *Electrochim. Acta*, 35(1990) 437.
8. R.N. Singh, J.P. Singh, B. Lal, M.J.K Thomas and S. Bera, *Electrochim Acta*, 51(2006) 5515.
9. W.K. Behl and J.E. Toni, *J. Electroanal. Chem*., 31(1971) 63.
10. L.D. Burke and M.M. Murphy, *J. Electrochem. Soc.*, 138(1991) 88.
11. H. Gomez Meier, J.R. Vilche and A.J. Arvia, *J. Electroanal. Chem*., 138(1982)367.
12. R.P. Šimpraga, *J. Electroanal. Chem*., 355(1993) 79.
13. T.-C. Liu, W.G. Pell and B.E. Conway, *Electrochim. Acta.*, 44(1999) 2829.
14. H. Gomez Meier, J.R. Vilche and A.J. Arvia, *J. Electroanal. Chem*., 134(1982) 251.
15. T. Ohtsuka and N. Sato, *J. Electroanal. Chem*., 147(1983) 167.
16. K.E. Heusler in *Passivity of Metals*, R.P. Frankenthal, J. Kruger, Eds., Electrochemical Soc. Inc. Princeton, New Jersey, 1978, p. 771.
17. A. Foelske and H.-H Strehblow, *Surf. Interf. Anal.*, 34(2002) 125.
18. L.D. Burke and E.J.M. O'Sullivan, *J. Electroanal. Chem*., 117(1981) 155.
19. L.D. Burke, M.I. Casey, V.J. Cunnane, O.J. Murphy and T.A.M. Twomey, *J. Electroanal. Chem*., 189(1985) 353.
20. L.D. Burke and M.E.G. Lyons, *J. Electroanal. Chem*., 198(1986) 347.
21. M.E.G. Lyons , M.P. Brandon, Phys.Chem.Chem.Phys., 2008, submitted for publication. Paper reference B815338H.
22. G.W. Simmons in *Passivity of Metals*, R.P. Frankenthal, J. Kruger, Eds., Electrochemical Soc. Inc. Princeton, New Jersey, 1978, p. 899.
23. D. Erts, E. Ahlberg, J. Asbjörnsson, H. Olin and J. Prikulis, *Appl. Phys.*, A66 (1998) S477.
24. R.N. Singh, J.-F. Koenig, G. Poillerat and P. Chartier, *J. Electrochem. Soc.*, 137(1990) 1408.
25. E.B.Castro, C.A. Gervasi and J.R. Vilche, *J. Appl. Electrochem.*, 28(1998) 835.
26. S. Palmas, F. Ferrara, A. Vacca, M. Mascia and A.M. Polcaro, *Electrochim. Acta.*, 53(2007) 400.
27. A.G.C. Kobussen, H. Willems and G.H.J. Broers, *J. Electroanal. Chem.*, 142(1982) 85.
28. M.E.G. Lyons, M.P. Brandon, *J. Electroanal. Chem., 2008*, paper in preparation.
29. D.A. Harrington and B.E. Conway, *Electrochim. Acta.*, 32(1987) 1703.
30. M.P. Brandon, Ph.D. Thesis, University of Dublin, Trinity College, 2008.

31. T. Kessler, J.R. Vilche, M. Ebert, K. Jüttner, and W.J. Lorenz, *Chem. Eng. Technol.*, 14(1991) 263.
32. G. Wu, N. Li, , D-R. Zhou, K. Mitsuo and B-Q. Xu, *J. Solid State Chem.*, 177(2004) 3682.
33. E.B. Castro, S.G. Real and L.F. Pinheiro Dick, *Int. J. Hydrogen Energy.*, 29(2004) 255.
34. K.K. Lian, D.W. Kirk and S.J. Thorpe, *J. Electrochem. Soc.*, 142(1995) 3704.
35. J.O'M. Bockris and T. Otagawa, *J. Phys. Chem.*, 87(1983) 2960.
36. R.E. Meyer, *J. Electrochem. Soc.*, 107(1960) 847.
37. J.J. MacDonald and B.E. Conway, *Proc. R. Soc. London, Ser. A*, 269(1962) 419.
38. D.S. Gnanamuthu and J.V. Petrocelli, *J. Electrochem. Soc.*, 114(1967) 1036.
39. V.I. Birss and A. Damjanovic, *J. Electrochem. Soc.*, 130(1983) 1688.
40. V.I. Birss and A. Damjanovic, *J. Electrochem. Soc.*, 130(1983) 1694.
41. V.I. Birss, A. Damjanovic and P.G. Hudson, *J. Electrochem. Soc.*, 133(1986) 1621.
42. V.I. Birss and A. Damjanovic, *J. Electrochem. Soc.*, 134(1987) 113.
43. A. Damjanovic, V.I. Birss and D.S. Boudreaux, *J. Electrochem. Soc.*, 138(1991) 2549.
44. N. Cabrera and N.F. Mott, *Repts. Prog. Phys.*, 12(1948-49) 163.
45. E.J.M. O'Sullivan and L.D. Burke, *J. Electrochem. Soc.*, 137(1990) 466.
46. L.D. Burke and M.E.G. Lyons, in *Modern Aspects of Electrochemistry, Vol. 18*, R.E. White, J.O'M. Bockris and B.E. Conway, Eds., Plenum Press, New York, 1986, p169.
47. S. Trasatti and O.A. Petrii, *Pure & Appl. Chem*., 63(1991) 711.
48. G.W.D. Briggs, in *Electrochemistry - Vol 4, Specialist Periodical Reports*, The Chemical Society, London, 1974, chapter 3, pp. 33-59.